THE UNIVERSITY of EDINBURGH

Edinburgh Research Explorer

Amyloid Beta and Tau Cooperate to Cause Reversible Behavioral and Transcriptional Deficits in a Model of Alzheimer's Disease

Citation for published version:
Pickett, EK, Herrmann, AG, McQueen, J, Abt, K, Dando, O, Tulloch, J, Jain, P, Dunnett, S, Sohrabi, S, Fjeldstad, MP, Calkin, W, Murison, L, Jackson, RJ, Tzioras, M, Stevenson, A, d'Orange, M, Hooley, M, Davies, C, Colom Cadena, M, Anton Fernandez, A, King, D, Oren, I, Rose, J, McKenzie, C-A, Allison, E, Smith, C, Hardt, O, Henstridge, CM, Hardingham, GE & Spires-Jones, TL 2019, 'Amyloid Beta and Tau Cooperate to Cause Reversible Behavioral and Transcriptional Deficits in a Model of Alzheimer's Disease', *Cell Reports*, vol. 29, no. 11, pp. 3592-3604.E5. https://doi.org/10.1016/j.celrep.2019.11.044

Digital Object Identifier (DOI):
10.1016/j.celrep.2019.11.044

Link:
Link to publication record in Edinburgh Research Explorer

Document Version:
Peer reviewed version

Published In:
Cell Reports

General rights
Copyright for the publications made accessible via the Edinburgh Research Explorer is retained by the author(s) and / or other copyright owners and it is a condition of accessing these publications that users recognise and abide by the legal requirements associated with these rights.

Take down policy
The University of Edinburgh has made every reasonable effort to ensure that Edinburgh Research Explorer content complies with UK legislation. If you believe that the public display of this file breaches copyright please contact openaccess@ed.ac.uk providing details, and we will remove access to the work immediately and investigate your claim.

OPEN ACCESS

Download date: 05. May. 2023

Amyloid beta and tau cooperate to cause reversible behavioural and transcriptional deficits in a model of Alzheimer's disease

Eleanor K Pickett[1], Abigail G Herrmann[1], Jamie McQueen[1,2], Kimberly Abt[1], Owen Dando[1,2], Jane Tulloch[1,2], Pooja Jain[1], Sophie Dunnett[1], Sadaf Sohrabi[1], Maria P Fjeldstad[1], Will Calkin[1], Leo Murison[1], Rosemary J Jackson[1,3], Makis Tzioras[1,2], Anna Stevenson[1,2], Marie d'Orange[1], Monique Hooley[1,2], Caitlin Davies[1,2], Marti Colom-Cadena[1,2], Alejandro Anton-Fernandez[1,2], Declan King[1,2], Iris Oren[1], Jamie Rose[1,2], Chris-Anne McKenzie[4], Elizabeth Allison[1], Colin Smith[4], Oliver Hardt[5,6], Christopher M Henstridge[1,7], Giles E Hardingham[1,2], and Tara L Spires-Jones[1,2,8]*

1. The University of Edinburgh Centre for Discovery Brain Sciences, 1 George Square, Edinburgh, EH8 9JZ UK
2. UK Dementia Research Institute at Edinburgh, George Square, Edinburgh, EH8 9JZ UK
3. MassGeneral Institute for Neurodegenerative Disease, Massachusetts General Hospital and Harvard Medical School, Charlestown, MA 02129 USA
4. Centre for Clinical Brain Sciences and Sudden Death Brain Bank, University of Edinburgh, Edinburgh EH16 4SB UK
5. McGill University Department of Psychology, Montreal QC H3A 1B1, Canada
6. The University of Edinburgh Simons Initiative for the Developing Brain, George Square, Edinburgh, EH8 9JZ UK
7. Current affiliation: University of Dundee School of Medicine, Dundee DD19SY
8. Lead contact

*Lead Contact/corresponding author: Prof Tara Spires-Jones, The University of Edinburgh Centre for Discovery Brain Sciences and UK Dementia Research Institute, 1 George Square Edinburgh EH8 9JZ UK, Tara.Spires-Jones@ed.ac.uk

Summary

One of the key knowledge gaps blocking development of effective therapeutics for Alzheimer's disease (AD) is the lack of understanding of how amyloid beta peptide (Aß) and pathological forms of the tau protein cooperate in causing disease phenotypes. Within a mouse tau deficient background, we probed the molecular, cellular and behavioural disruption triggered by wild-type human tau's influence on human Aß-induced pathology. We find that Aß and tau work cooperatively to cause a hyperactivity behavioural phenotype and to cause downregulation of transcription of genes involved in synaptic function. In both our mouse model and in human post-mortem tissue, we observe accumulation of pathological tau in synapses, supporting the potential importance of synaptic tau. Importantly, tau reduction in the mice initiated after behavioural deficits emerge was found to correct behavioural deficits, reduce synaptic tau levels, and substantially reverse transcriptional perturbations, suggesting that lowering synaptic tau levels may be beneficial in AD.

Introduction

Over 50 million people are living with dementia today, and approximately $800 billion per year is spent worldwide on their health and social care (Prince et al., 2015). Alzheimer's disease (AD) is the most common cause of dementia, and current treatments are only minimally effective and do not prevent brain degeneration or cognitive decline. AD is defined pathologically by the accumulation of amyloid plaques made of aggregated amyloid beta (Aß), neurofibrillary tangles which are intraneuronal deposits of hyperphosphorylated tau protein, and brain atrophy due to neuron and synapse loss. The predominating hypothesis in the AD field, the amyloid cascade hypothesis, posits that changes in Aß initiate a cascade of events including pathological changes in tau (Hardy and Higgins, 1992, Hyman, 2011). Genetic studies indicate that changes in the innate immune system are also important in conferring disease risk (De Strooper and Karran, 2016, Henstridge et al., 2019). How Aß, glial/innate immune changes, and tau interact to cause neurodegeneration remains a key knowledge gap in the field.

Synapses are an important target to study in AD as synapse degeneration is the strongest correlate of cognitive decline (Terry et al., 1991) and synapses are important early in disease pathogenesis and the spread of pathological proteins through the brain (Spires-Jones and Hyman, 2014, Spires-Jones et al., 2017, DeVos et al., 2018b). Substantial amounts of evidence implicate oligomeric Aß in synapse degeneration in model systems and in human post-mortem tissue (Li et al., 2009, Mucke and Selkoe, 2012, Klein, 2013, Spires et al., 2005, Spires-Jones et al., 2007, Spires-Jones et al., 2009, Koffie et al., 2009, Koffie et al., 2012, Jackson et al., 2019). Some of the toxic effects of Aß appear to be mediated by cascades which are normally involved in the innate immune system including complement and TREM2 (Hong et al., 2016, Jay et al., 2017, Yeh et al., 2016, Henstridge et al., 2019). Pathological forms of tau are also sufficient to induce synapse loss and circuit dysfunction in models of tauopathy (Kopeikina et al., 2012, Menkes-Caspi et al., 2015, Crimins et al., 2013, Fox et al., 2011, Hoover et al., 2010, Zhou et al., 2017, Busche et al., 2019).

There is accumulating evidence that Aß and tau may act synergistically to cause synaptic dysfunction, neurofibrillary tangle mediated neuron loss, and behavioural deficits (Ittner et al., 2010, Vargas-Caballero et al., 2017, Roberson et al., 2011, Shipton et al., 2011, Jackson et al., 2016, DeVos et al., 2018a). However, much of the previous work was confounded by the complex differences between mouse and human tau and the inability to control tau expression. Further, many of the previous studies examining interactions between Aß and tau used tau mutations associated with frontotemporal dementia to drive neurofibrillary

pathology. While these are excellent models for studying tau pathology, they do not accurately recapitulate the state in early AD in which soluble, wild-type human tau is likely interacting with rising levels of oligomeric Aß to confer synaptic toxicity. To overcome these limitations, and test the hypothesis that Aß and tau act cooperatively to cause behavioural and transcriptional deficits, we designed a model lacking endogenous mouse tau (MAPTnull) and expressing both the APP/PS1 transgene, which causes well-characterized plaque-associated synapse loss (Jankowsky et al., 2004, Koffie et al., 2009), and the rTg21221 line which reversibly expresses wild-type human tau under the control of an inducible promotor (Hoover et al., 2010). This MAPTnull+APP/PS1+rTg21221 AD model (APP/PS1+Tau) allows control over tau levels by suppression of tau transgene expression. We examined the behaviour, pathology, synapse degeneration, transcriptional changes and accumulation of Aβ and tau at synapses in the APP/PS1+Tau model and compared these data to observations of synapses in human post-mortem brain using the high-resolution array tomography imaging technique (Kay et al., 2013).

Results

APP/PS1+Tau mice develop age-related behavioural and transcriptional phenotypes

To understand the effects of combining plaque pathology with human tau expression, we examined pathology and behaviour during ageing in APP/PS1+Tau mice and 3 littermate control genotypes: control (MAPTnull), APP/PS1 only (MAPTnullxAPP/PS1), and human tau only (MAPTnullxrTg21221, Fig. 1A,B). Pathological and behavioural data for each mouse are found in table S1. APP/PS1+Tau mice develop progressive amyloid plaque pathology in the absence of tau pathology (Fig. 1C-E). Similar to previous data for the rTg21221 line (Hoover et al., 2010), APP/PS1+Tau mice over express human tau ~12-fold compared to endogenous mouse tau levels seen in wild-type mice by qPCR (human and mouse tau normalized to GAPDH, n=5 per group, data not shown). In both genotypes of mice expressing the APP/PS1 transgene, amyloid plaques begin to appear in cortex and hippocampus by 6 months of age and plaque burden increases with age. Plaque deposition differs between APP/PS1 mice and APP/PS1+Tau mice with surprisingly lower plaque in APP/PS1+Tau mice (Fig. 1D). Although human tau mRNA and protein could be detected in the two genotypes expressing both the human tau responder gene and the CkTta activator transgene, no tau pathology was observed at any age with staining for phosphorylated or misfolded tau epitopes (AT8, PHF1, Alz50) or with histological staining of fibrils with thioflavin S (Fig. 1E). The efficacy of tau staining was confirmed using rTg4510 mouse brain sections (which express a form of tau associated with frontotemporal dementia and contain tangle pathology), verifying that all tau antibodies stained neurofibrillary tangles. APP/PS1+Tau mice did not exhibit age-related atrophy in cortex (Fig. 1F) or

hippocampus (Fig. S1).

In addition to plaque accumulation and human tau expression, APP/PS1+Tau mice exhibit an age-related hyperactivity phenotype (Fig. 2A,B). After 3 days of habituation, mice were placed in an open field and the total distance travelled over 10 minutes was recorded. Two-way ANOVA reveals a significant effect of genotype ($F[3,202]=314.76$, $p<0.0001$) with APP/PS1+Tau mice travelling further than controls at 10.5 and 14.5 months of age (Tukey's multiple comparisons test $p<=0.01$ for all comparisons of APP/PS1+Tau vs other 3 genotypes at 10.5 and 14.5 months). There was no effect of age when all mice were considered together ($F[4,202]=1.61$, $p=0.17$) but there was a significant interaction between age and genotype ($F[12,202]=2.30$, $p=0.01$) due to the APP/PS1+Tau mice travelling further in the open field than the other genotypes as they age. The hyperactivity phenotype is not different in male vs female APP/PS1+Tau mice (Fig. S2). Neither is the hyperactivity driven by tau protein levels which do not differ between APP/PS1+Tau mice and tau mice as measured by ELISA in cortical homogenates from 14.5 month old mice (mean 11.0 ng/mg total protein in tau mice, 9.5 ng/mg total protein in APP/PS1+Tau mice n=5 per group, $p>0.05$ Tukey's post hoc test). Group sizes and sex of mice in behavioural studies are shown in figures and in table S1.

To examine transcriptional changes in APP/PS1+Tau mice, we performed unbiased RNA-seq on brain homogenates at 14.5 months of age (RNAseq data found in table S2). When compared to control mice, APP/PS1 had 81 transcripts that changed more than 2 fold and had an adjusted p value of less than 0.05 (Fig. 2C). Tau mice were very similar to controls with only 6 transcripts significantly changing more than 2 fold, one of which is *Mapt* which is expected due to tau overexpression (Fig. 2D). In contrast, APP/PS1+Tau mice had 1531 transcripts which were significantly altered compared to MAPTnull control mice and 127 of these were changed by greater than 2 fold (Fig. 2E). Thus, the gene changes in APP/PS1+Tau mice compared to control are much larger than either APP/PS1 mice or Tau mice, indicating cooperation between Aβ and tau in causing transcriptional dysregulation. Ingenuity Pathway Analysis indicates that many of the upregulated genes in APP/PS1+Tau mice are typically expressed in glia (summary pathways of interest based on the literature shown in Fig. 2G, full pathway analyses in table S3). This includes increased expression of *Trem2, Gfap, Cd68, C1q*, and *H2-Eb1* and significant increases in canonical pathways implicated in neuroinflammation (Fig 2G). Many of the downregulated genes in APP/PS1+Tau mice are involved in canonical pathways involved in synaptic function including glutamate receptor signalling and calcium signalling (AMPA and NMDA receptor subunits, *Gria2, Gria3,*

Gria4, Grin2a, Homer2 and *Camk2b* are downregulated, Fig 2G). One synaptic transcript that was significantly upregulated is cellular prion protein (*Prnp*), which is very interesting since it is a known synaptic binding partner of Aß (Um et al., 2012).

Upregulation of genes in APP/PS1+Tau mice appears to be largely driven by Aß and tau independently without an additive effect since the fold induction of upregulated genes is very similar in APP/PS1+Tau mice to the maximum fold induction in either APP/PS1 or Tau mice. Most of the upregulated transcripts in APP/PS1+Tau mice correlate strongly with the maximum fold change in APP/PS1 mice (Fig. 2F), and most upregulated pathways in APP/PS1+Tau mice are upregulated to a similar extent in APP/PS1 mice (Fig.2G). There are a few pathways upregulated more in APP/PS1+Tau mice than in APP/PS1 or Tau mice including the complement system (Fig. 2G). In contrast to the relatively few changes seen in upregulated genes, Aß and tau act additively in downregulating gene expression. The fold downregulation compared to controls in APP/PS1+Tau mice is more than the maximum change in either APP/PS1 mice or Tau mice (Fig. 2F). Interestingly, pathway analysis reveals the glutamate receptor signalling pathway is significantly decreased in APP/PS1+Tau mice compared to controls and unaffected in either parent line (Fig 2G). One potential mechanistic link between upregulated inflammatory pathways and synaptic dysfunction and decreases in synaptic gene expression is the phagocytosis of synaptic proteins by microglia. The complement system has been previously shown to be involved in phagocytosis of synapses in plaque and tangle bearing models separately (Dejanovic et al., 2018, Hong et al., 2016, Litvinchuk et al., 2018, Shi et al., 2017). In addition to upregulation of genes involved in the complement system and downregulation of genes involved in synaptic function in APP/PS1+Tau mice, we observe synaptic phagocytosis by microglia (Fig 2H).

Cooperative effects of Aβ and tau on behaviour and transcription are ameliorated by lowering tau levels in APP/PS1+Tau mice

To determine whether the phenotypes observed in APP/PS1+Tau mice could be ameliorated by lowering tau levels, a cohort of mice were treated with doxycycline (dox) from 10.5 to 14.5 months to suppress tau transgene expression. Dox treatment lowered tau expression by 65% in APP/PS1+Tau mice (Fig 3A). While this lowering of human tau levels was not complete and remained higher than endogenous mouse tau levels would be in a wild-type mouse, it completely ameliorated the hyperactivity phenotype in APP/PS1+Tau mice (Fig. 3B,C). Doxycycline treatment also ameliorates gene expression changes in APP/PS1+Tau mice (Fig. 3D,E) and reverses the mild changes in Tau mice (Fig. S3), indicating that

lowering tau levels protects against gene expression changes. Pathway analysis reveals a striking amelioration of the top 15 most up and down regulated networks in APP/PS1+Tau mice treated with dox (Fig. 3E).

To test whether the recovery of gene expression with tau suppression was due to a prevention of further changes with age or a recovery of existing changes at the time treatment began, we analysed a subset of transcripts by RT-PCR at 9-10 months of age (an age before treatment started) and validated the RNA-seq data with RT-PCR in 14.5 month old brain samples that had been treated with vehicle or dox. The subset of genes tested indicate that the amelioration of gene expression changes with dox was due to a prevention of further worsening and not a recovery (Fig. S3). Since many of the upregulated inflammatory genes are expressed in glia, we examined astrocyte and microglial burdens. In agreement with the RNA-seq observation that upregulated genes are driven largely by Aß without an additive effect of tau, an increase in gliosis was observed in both genotypes with human Aß, APP/PS1+Tau and APP/PS1 mice. The burden of gliosis did not recover with dox treatment, however many of the inflammatory markers expressed by glia were reduced with tau suppression, which may contribute indirectly to the recovery of the levels of synaptic genes involved in glutamatergic signalling (Fig 3E). In particular, the increases in transcripts involved in the complement system are normalized by dox treatment (Fig. S3), which is of interest due to the recent links between complement and pruning of synapses in mice expressing frontotemporal dementia associated mutant tau (Dejanovic et al., 2018, Litvinchuk et al., 2018).

To examine whether the increased distance travelled by APP/PS1+Tau mice was due to anxiety, we examined the distance travelled in the inner versus outer portions of the arena. Mice of all genotypes spend approximately 10 times more time in the outer than inner arena indicating a typical avoidance of open areas (Fig. S2). At 14.5 months of age (after treatment), there was no significant effect of genotype or treatment on distance travelled in the inner arena (2-way ANOVA genotype $F[3,69]=1.854$, treatment $F[1,76]=0.204$, interaction $F[2,69]=0.153$, $p>0.05$). In the outer arena, there were significant effects of genotype, treatment, and an interaction between genotype and treatment on distance travelled. APP/PS1+Tau vehicle treated mice travelled significantly further in the outer arena than all other groups. This indicates a potential anxiety phenotype as well as hyperactivity, which recovers with doxycycline treatment.

Tau in synapses may mediate behavioural and transcriptional changes

To examine the brain changes underpinning the recovery of behaviour with tau suppression, post-mortem studies of pathological and molecular changes were carried out in the cohort of mice that had undergone treatment. Amyloid plaque pathology is unchanged with tau suppression (Fig. S4). The ThioS plaque burden, cross sectional area of individual ThioS stained plaques, AW7 immunostained plaques (which label both the dense core and oligomeric halo surrounding the core), and the area of the oligomeric Aß halo surrounding plaques were all unchanged with dox treatment. Expression of APP measured by qPCR was increased in APP/PS1+Tau mice compared to APP/PS1 littermates and this increase was ameliorated by tau transgene suppression. Soluble levels of Aß 42 peptide however, were not different in APP/PS1+Tau mice compared to APP/PS1 mice, and although there was a significant effect of treatment across groups, post-hoc tests show no difference between APP/PS1+Tau vehicle and dox treated mice in Aß 42 levels (Fig. S4). These data indicate that the behavioural and gene transcription recovery was not mediated by reducing amyloid pathology.

Synapse density around plaques and the accumulation of synaptic Aß and tau were determined in entorhinal cortex using array tomography. More than 673,000 postsynaptic densities labelled with PSD95 and 415,000 presynaptic terminals labelled with synaptophysin were analysed from cortical samples from 4-11 mice per group (average 13,000 PSDs and 9,655 presynaptic puncta per mouse). Density of both synaptophysin (Fig 4) and PSD95 (Fig. S5) labelled puncta was decreased near plaques in the two genotypes that have plaques (APP/PS1 and APP/PS1+Tau mice, 3-way ANOVA effect of plaque distance synaptophysin $F[1,42]=60.49$, $p<0.0001$, PSD95 $F[1,50]=8.15$, $p=0.006$). Treatment with doxycycline to reduce tau levels did not prevent this plaque-associated synapse loss. The density of pre and post synapses near plaques was not significantly different between treatment groups or genotypes. Oligomeric Aß accumulated in a subset of synapses near plaques in both APP/PS1 and APP/PS1+Tau mice (median presynaptic terminals near plaques containing Aß 1.9% in APP/PS1 mice, 0.8% in APP/PS1+Tau mice; median postsynaptic terminals 1.0% in APP/PS1 mice, 2.4% in APP/PS1+Tau mice). The percentage of both pre and postsynaptic terminals containing Aß was higher near plaques in both APP/PS1 and APP/PS1+Tau mice (independent samples Mann-Whitney U test PSD95 $p<0.01$, synaptophysin $p<0.0001$ for all groups near vs far from plaques). The percentage of synapses containing Aß near plaques was not different between APP/PS1 and APP/PS1+Tau mice (independent samples Mann-Whitney U test $p>0.05$). There was also no effect of lowering tau levels on accumulation of Aß in synapses near plaques (independent samples effect of treatment, Mann-Whitney U test $p>0.05$).

Tau was detected in median of 0.4% of presynapses (Fig.4E) and 1.2% of PSDs (Fig. S5) in vehicle treated APP/PS1+Tau mice and 1.1% of presynapses and 0.6% of PSDs in vehicle treated Tau mice. Tau was not detected in synapses in mice that did not express tau (control and APP/PS1). Unlike Aß, the percentage of synapses containing tau was not different near plaques in the APP/PS1+Tau group. The percentage of synapses containing tau were significantly different between genotypes (independent samples Mann-Whitney U test for genotype $p<0.0001$). Doxycycline treatment significantly lowered synaptic tau levels only in the APP/PS1+Tau group (data split by genotype, effect of treatment independent samples Mann-Whitney U test $p=0.004$ for PSD95, $p=0.004$ synaptophysin). The approximate 30-fold reduction in presynaptic and 8-fold reduction in postsynaptic tau levels in APP/PS1+Tau mice may contribute to the improved hyperactivity phenotype and ameliorated transcriptional profiles observed in mice treated with doxycycline. However this will need to be confirmed in future studies as treatment lowered tau levels globally, not just in synapses. Only very rare PSDs stained for both Aß and tau (<0.006% of pre <0.005% post synapses in vehicle treated APP/PS1+Tau mice).

Tau is present in pre and post synapses of human AD cases

To confirm the translational relevance of the contribution of synaptic tau to cognitive decline in our model, we examined the localization of tau and Aß at synapses in samples of superior temporal gyrus from human subjects. In total 99,967 postsynapses and 100,012 presynapses from 6 AD and 6 control subjects were examined (mean 8,331 post and 8,334 presynapses examined per case, data found in table S4). Cases were stained with the pan-Aß antibody AW7, a total tau antibody, a presynaptic marker, and a postsynaptic marker in a two-day protocol to allow localization of Aß and tau together within individual pre and postsynapse. As previously reported, Aß is present in a subset of synapses in AD brain (Koffie et al., 2012, Jackson et al., 2019). In this cohort we again observe significantly more positive synapses within 20 μm of a plaque (median 10.4% PSD and 8.0% synaptophysin puncta positive for Aß near plaques, <1% PSD or synaptophysin positive for Aß far from plaques, $p<0.05$ Independent samples Mann-Whitney U test for both pre and post synapses). In array tomography, the tau13 antibody recognized neurofibrillary pathology but not normal axonal tau, and labelled a small subset of pre and post-synapses (Fig. 5). As observed in the mice, tau synaptic localization was not different near versus far from plaques. Also in agreement with the mouse data, only very rare synapses were positive for both tau and Aß staining (<0.02% on average). Misfolded and phosphorylated tau were also detected in human synapses using array tomography staining with Alz50, MC1, and CP13 antibodies (Fig. 5G-J).

Discussion

The lack of disease modifying treatments for AD remains a huge unmet clinical need. Synapse degeneration is the strongest pathological correlate of cognitive decline in AD and a potentially important driver of disease pathogenesis. Previous work by our group and others strongly implicated soluble Aß and tau separately in synapse dysfunction and loss in AD (Spires-Jones and Hyman, 2014, Klein, 2013, Koffie et al., 2012, Koffie et al., 2009, Kopeikina et al., 2012, Mucke and Selkoe, 2012, Spires-Jones et al., 2017). Here we tested the hypothesis that Aß and tau act together to cause neural circuit dysfunction. Evidence has been growing to support this idea from work showing that lowering tau levels protects against Aß mediated synaptic plasticity deficits, from studies indicating that dendritic tau mediates Aß synaptotoxicity, and from a study that found synaptic tau phosphorylation in APP/PS1 mice (Roberson et al., 2011, Shipton et al., 2011, Roberson et al., 2007, Ittner et al., 2010, Zempel et al., 2010, Wu et al., 2018). Recent work in a mouse model expressing both APP/PS1 and P301L mutant tau which is associated with frontotemporal dementia showed that reducing levels of mutant tau prevents neuronal loss (DeVos et al., 2018a). In our APP/PS1+Tau model, the tau expressed is wild-type human tau without endogenous mouse tau making this relevant to early Alzheimer's disease.

In this APP/PS1+Tau model, we observe an age-related hyperactivity phenotype and downregulation of genes involved in synaptic function. Pathologically, we observe tau in both pre and post synapses in human brain and in our APP/PS1+Tau model. Tau was very rarely colocalised with Aß within individual synapses. Reducing tau expression levels ameliorated the behavioural and gene expression phenotypes and lowered synaptic tau levels without recovering synapse density around plaques. Importantly, doxycycline treatment of our mice did not completely remove human tau indicating that a partial reduction in tau levels may be sufficient in humans to allow some functional recovery. This may be more achievable than complete knockdown and could also preserve physiological functions of tau. Together, these data support the hypothesis that Aβ and tau act together to cause synapse dysfunction. However, this interaction is not likely to be due to physical colocalization of small aggregates of these pathological proteins within the same synapses, at least within the limits of our detection.

We surprisingly observed that human tau expression in the absence of mouse tau resulted in smaller plaques in APP/PS1+Tau mice, whereas we previously saw that adding human tau with the same transgenic line when endogenous mouse tau is still present resulted in slightly larger plaques (Jackson et al., 2016). This implies that either mouse and human tau function differently in mouse brain, that the

overexpression of human tau results in different effects than endogenous levels of mouse tau, or that the temporal and spatial expression pattern driven by the CamKIIα promotor does not recapitulate accurately the physiological expression of endogenous tau. Together these data highlight the importance of examining multiple models including knock-in lines (Sasaguri et al., 2017) and of using human post-mortem tissue as well as mouse models to ensure the translatability of findings.

Potential molecular mechanisms linking Aß and tau to synapse and circuit dysfunction include calcium dysregulation and calcineurin activation, which are known to contribute to Aß toxicity and spine collapse *in vitro* and *in vivo* and have been linked to tau mediated synapse impairment (Wu et al., 2010, Hudry et al., 2012, Kuchibhotla et al., 2008, Mattson et al., 1992, Zempel et al., 2010, Yin et al., 2016). Human tau expression further causes circuit hypoactivity, even in APP/PS1 mice which usually exhibit hyperactive neurons (Busche et al., 2019). These data are in line with our current study as both show cooperativity between Aβ and tau in impairing neuronal activity and circuit function.

Abnormal activation of synaptic receptors by Aß has also been shown to induce activation of kinases including Fyn and GSK3-ß which affect tau phosphorylation and synapse collapse (Purro et al., 2012, Lovestone et al., 2014, Small and Duff, 2008, Marzo et al., 2016, Sellers et al., 2018, Ittner et al., 2010, Roberson et al., 2011). Our RNA-seq results add to the literature implicating cellular prion protein at the interface between Aß and tau as increases in PrPc mRNA in APP/PS1+Tau mice was the largest change observed with RNA-seq and these levels recover with tau suppression. PrPc has been shown to interact with oligomeric Aß where it is thought to act via metabotropic glutamate receptor 5 complexes to impair synaptic function (Haas and Strittmatter, 2016, Jarosz-Griffiths et al., 2016, Barry et al., 2011, Hu et al., 2018, Hu et al., 2014). This pathway could involve tau since binding of Aß to PrPc can activate Fyn and cause tau phosphorylation (Um et al., 2013, Um et al., 2012). While many of the proposed mechanisms of synapse degeneration focus on postsynaptic processes, our data clearly show accumulation of both Aß and tau in pre as well as postsynaptic terminals. Tau has recently been shown to bind to presynaptic vesicles in human AD and Drosophila models, where it impairs neurotransmitter release (Zhou et al., 2017, McInnes et al., 2018). Similarly, it is also becoming clear that Aß exerts effects on presynaptic function (Ovsepian et al., 2018).

Our RNA-seq results strongly implicate non-neuronal cells as key participants in the interplay between Aß and tau, which is of interest in the field (Henstridge et al., 2019). TREM2, clusterin, and CD33, genes involved in the innate immune system that have been implicated in AD risk by GWAS studies, were

elevated in APP/PS1+Tau mice compared to controls. Several members of the complement cascade family were also changed in APP/PS1+Tau mice, which is important due to the recent discovery of complement mediated microglial engulfment of synapses in plaque bearing AD model mice (Hong et al., 2016, Shi et al., 2017). Previous data on transcriptional changes in amyloid models compared to tau models demonstrated that changes in immune gene expression correlated positively with amyloid pathology and decreases in synaptic gene expression correlated with neurofibrillary tangle pathology (Matarin et al., 2015). Our data indicate that beyond contributing to disease risk, presumably through amyloid, the innate immune system is also likely involved in the cascade from amyloid to tau in AD pathogenesis. The gene changes observed in our model indicate that Aß and tau act cooperatively to cause downregulation of genes and largely independently in gene upregulation. Downregulated genes were predominantly involved in excitatory synaptic function, which is supported by recent data implicating tau in toxicity to excitatory over inhibitory neurons (Fu et al., 2017).

We propose that the inflammatory milieu initiated by amyloid primes the system making synapses vulnerable to tau-associated molecular changes such as loss of synaptic proteins. In the absence of amyloid pathology, our tau expressing mice do not develop loss of synaptic protein expression or behavioural abnormalities despite accumulation of tau in synapses, whereas APP/PS1+Tau mice have synaptic tau in the context of an inflammatory reaction to Aß which could drive behavioural phenotypes and loss of synaptic proteins. Interestingly, recent work in mice expressing dementia-associated mutant tau indicates that the complement system is involved in neurodegeneration, however reducing microglial numbers by inhibiting CSF1R did not ameliorate degenerative phenotypes (Bennett et al., 2018, Dejanovic et al., 2018, Litvinchuk et al., 2018). Thus while mutant tau may be sufficient to induce inflammatory phenotypes that contribute to degeneration in mice, in the context of Alzheimer's disease, it may be that amyloid induces inflammatory changes which exacerbate degeneration when tau is present. Our data also suggest that synaptic proteins may be cleared at least in part by microglial phagocytosis.

Synapses are highly plastic structures, which have the potential for recovery with interventions. Indeed, most successful drugs used in nervous system disorders act at the synapse; therefore synaptic changes are an obvious target for disease-modifying agents in neurodegenerative disorders. Recent work has focused on removing Aß from synaptic receptors as a therapeutic avenue. For example, a compound that displaces Aß from sigma-2 receptors is now in clinical trials (Izzo et al., 2014, Grundman et al., 2019), (clinicaltrials.gov/ct2/show/NCT03507790). Our data indicate that lowering pathological tau or blocking the inflammatory changes that may link amyloid and tau toxicity may also be effective therapeutic

strategies.

Acknowledgements

We thank our human brain tissue donors and their families for their valuable contributions to this work. Many thanks also to Prof George Carlson and Ms Rose Pitstick for their input on mouse breeding and providing mouse lines and to Dominic Walsh and Peter Davies for providing antibodies. This work was funded by the UK Dementia Research Institute which receives its funding from DRI Ltd, funded by the UK Medical Research Council, Alzheimer's Society, and Alzheimer's Research UK, the European Research Council (ERC) under the European Union's Horizon 2020 research and innovation programme (Grant agreement No. 681181), Alzheimer's Research UK and the Scottish Government Chief Scientist Office (ARUK SPG2013-1), a Wellcome Trust-University of Edinburgh Institutional Strategic Support Fund, MND Scotland, and Alzheimer's Society. SD contributed to this work funded by an Alzheimer's Society summer studentship. MF contributed to this work funded by a summer studentship from Medical Research Scotland. TSJ gratefully acknowledges affiliations with the Centre for Dementia Prevention, the Euan MacDonald Centre, and Edinburgh Neuroscience. Two of the control participants in the human study were from the Lothian Birth Cohort 1936, thus we wish to thank the cohort and research team supported by Age UK (Disconnected Mind project) in The University of Edinburgh Centre for Cognitive Ageing and Cognitive Epidemiology, funded by the Biotechnology and Biological Sciences Research Council (BBSRC) and Medical Research Council (MRC) ((MR/K026992/1). We acknowledge that the graphical abstract was created with Biorender software.

Author Contributions

Conceptualization, G.H. and T.L.S-J.; Methodology, E.K.P., J.T., G.A.C., and T.L.S.-J., Software, T.L.S.-J., M.C.C. and E.A.; Formal Analysis, O.D., M.H., I.O. G.E.H. and T.L.S.-J.; Investigation, E.K.P., J.M., K.A., J.T., A.G.H., P.J., S.D., S.S.S., A.S., M.F., W.C., L.M., R.J.J., M.T., M.D'O., J.R., R.P., C.-A.M., M.C.C., A.A., C.S., and C.M.H; Writing – Original Draft, E.K.P, and T.L.S.-J.; Writing – Reviewing & Editing, C.M.H, G.H., and T.L.S.-J.; Supervision, I.O., O.H., G.H., and T.L.S.-J.; Funding Acquisition G.H., and T.L.S.-J.

Declaration of interests

T.L.S-J. receives funding from 3 industry collaborators and is on the Scientific Advisory Board of Cognition Therapeutics. None of these companies had any influence over the current work.

FIGURE LEGENDS

Fig. 1. Progressive plaque pathology without tau pathology in APP/PS1+Tau mice. The APP/PS1+Tau mouse model was generated by breeding two feeder lines to produce four experimental genotypes of F1 littermates on a consistent outbred strain background (A). Behavior, pathology, and recovery with tau transgene suppression were characterized over time (B). Staining with Thioflavin S (C) shows progressive plaque accumulation in APP/PS1+Tau and APP/PS1 mice. APP/PS1+Tau mice have significantly lower cortical plaque burden than APP/PS1 mice (D, 2 way ANOVA effect of genotype $F[2,26]=8.454$, $p=0.007$). Tau is present in 14.5 month old APP/PS1+Tau mice as shown with a total tau stain, but tau pathology does not accumulate in cell bodies or in dystrophic neurites around plaques as shown by staining with phospho-tau (PHF1 and AT8), or misfolded tau (Alz50) antibodies, which all label tangle pathology in rTg4510 positive control sections (E). None of the genotypes experienced age related cortical atrophy (F, 2-way ANOVA effect of age, $p>0.05$). Data shown are means +/- standard error. Dots on bar graphs represent means of individual animals (n per group, biological replicates, shown in each bar). Scale bars represent 1mm (c, insets 100x100 µm), 30 µm (e). See also Figure S1 and table S1.

Fig. 2: Hyperactivity and transcriptional changes in APP/PS1+Tau mice. The open field test was used as a measure of spontaneous activity. Representative traces from a mouse from each genotype at 10.5 months of age (A), demonstrate the excess activity of the APP/PS1+Tau mice compared to the other three genotypes (B, Two-way ANOVA effect of genotype ($F[3,202]=314.76$, $p=0<0.0001$, * Tukey's post hoc tests $p<=0.01$ all comparisons of APP/PS1+Tau vs other 3 genotypes at 10.5 and 14.5 months, n of mice as biological replicates per group are noted on the graph). Dotted line in B indicates a different cohort of mice was used at 3-6-9 and 10.5-14.5 months. RNA-seq of APP/PS1 brain compared to controls reveals significant changes in gene expression (C, FPKM, Fragments Per Kilobase of transcript per Million mapped reads, biological replicates were mice, n=5 per group). Wild-type human tau induced changes to a lesser extent (D). APP/PS1+Tau mice (E) had more significant changes than when either APP/PS1 or Tau were expressed on their own. Transcripts changed more than 2 fold with an adjusted p value of $p<0.05$ are shown in red in panels C-E. A few transcripts of interest based on previous work are labelled with gene names. Examining only the genes significantly changed in APP/PS1+Tau mice compared to control mice and comparing the log(2) fold change (L2FC) of these on the x-axis to the maximum L2FC of either APP/PS1 or Tau compared to controls on the y axis (F) shows that upregulated genes are for the most part not differentially regulated in APP/PS1+Tau mice compared to those expressing APP/PS1 or tau alone (black line linear regression slope 0.90, 95% CI 0.89 to 0.92, dotted red line is x=y showing expected values if there were no differences). Downregulated genes in APP/PS1+Tau mice (F) are differentially regulated in APP/PS1+Tau mice compared to those expressing APP/PS1 or tau alone (black line linear regression slope 0.57, 95% CI 0.51 to 0.63). Green crosses in F show transcripts of interest which are changed more in APP/PS1+Tau mice than in APP/PS1 or Tau mice including downregulated genes involved in synaptic function and upregulated genes involved in inflammation. Each cross in C-F represents the average value of 5 mice per genotype of a single transcript detected at >1 FKPM. Pathway analysis of all RNAseq data (G) reveals that many of the upregulated pathways in APP/PS1+Tau mice are also upregulated in APP/PS1 mice and most downregulated pathways are also downregulated in Tau mice (orange indicates increases, blue decreases compared to control levels, analysis from Ingenuity Pathway Analysis software). However, there are pathways changed more in the APP/PS1+Tau line compared to the parent lines including increases in the complement system and decreases in glutamatergic signalling. Confocal imaging of Iba1 and synaptophysin staining shows that microglia engulf synaptic proteins around plaques (H, arrows show localization of synaptophysin inside microglia). Scale bar shows 5 microns. See also Figure S2 and tables S1-S3.

Fig. 3: Lowering tau levels ameliorates hyperactivity phenotype and transcriptional changes. Transgene suppression (dox) reduced human tau mRNA levels by approximately 65% as measured by qPCR (A, * 2-way ANOVA effect of treatment $F[1,31]=42.22$, $p<0.0001$). Representative traces of open field activity from a APP/PS1+Tau mouse treated with vehicle and one treated with doxycycline and the trace from the same mice after treatment (B) shows a clear amelioration of hyperactivity phenotype in one mouse which is confirmed by quantification of distance travelled (C, repeated measures ANOVA effect of genotype $F(3,69)=34.12$, $p<0.0001$, effect of treatment $F[1,69]=6.75$, $p=0.01$, interaction $F[3,69]=6.13$, $p=0.001$); *Tukey's multiple comparisons tests dox treated APP/PS1+Tau mice are significantly different from vehicle treated APP/PS1+Tau mice at 14.5 months of age ($p<0.0001$)). RNA-seq data show that dox treatment to reduce tau levels reverses transcriptional changes in APP/PS1+Tau mice (D, linear regression slope = -0.34, 95% CI -0.36 to -0.33). Each point represents a single transcript (average of n=5 mice per group). Pathway analysis reveals that the top 15 up and downregulated canonical pathways in APP/PS1+Tau mice compared to controls recover to normal levels or past normal levels with dox treatment (E, orange indicates increases, blue decreases compared to control levels, analysis from Ingenuity Pathway Analysis software). Biological replicates/experimental unit for each experiment is an individual mouse, n per group shown on the panels A and C. See also Figures S3 and S4 and tables S1-S3.

Fig. 4: Tau suppression reduces presynaptic accumulation of tau in entorhinal cortex. To investigate synapse loss and synaptic proteins, array tomography ribbons from 14.5 month old mice were stained for presynaptic terminals (synaptophysin, green) human tau (red), and amyloid beta (AW7, cyan). Maximum intensity projections of 10 serial 70 nm sections of a mouse in each group are shown in A. Three-dimensional reconstructions of 5 consecutive serial sections from processed image stacks of a APP/PS1+Tau mouse (B) demonstrate presynaptic terminals positive for tau (arrows) or Aß (arrowheads). Quantification reveals significant presynapse loss near plaques in APP/PS1 and APP/PS1+Tau mice which is not rescued by lowering tau levels with doxycycline (dox) treatment (C). The percentage of presynapses positive for Aß is not different between MAPTnullxAPP/PS1 mice and APP/PS1+Tau mice, nor is it affected by dox treatment (D). The percentage of presynapses containing tau is significantly lowered by dox treatment in APP/PS1+Tau mice (e, * Mann-Whitney U test $p=0.004$). Data represent mean + SEM (C) and median + interquartile range (D,E). Scale bars represent 10 μm in A, 1 μm in B. Each dot on the graphs represents the mean (C) or median (D,E) of a single mouse (biological replicate/experimental unit = mouse, n's shown on each panel). See also Figure S4 and S5 and table S1.

Fig. 5: Tau is found in pre and postsynapses in human AD brain. Array tomography was used in human AD and control postmortem brain tissue to stain Aß (white), Tau13 (yellow), PSD95 (magenta), and synaptophysin (cyan) (A-D). Tau13 stains neuropil threads (arrows, A). Examining individual synapses revealed that Aβ was present in 8.0% of presynaptic terminals (B, arrowheads) and 10.4% of postsynaptic densities (B arrows) near plaques in AD cases (B,E). Tau13 staining was observed in 0.23% of presynaptic terminals (arrowheads C, quantified in F), and 0.32% of postsynaptic terminals (arrows,D quantified in F). Misfolded tau labeled with Alz50 (G-I, yellow) was also observed in neuropil threads (arrows G) and in presynapses (arrowheads, H) and post synapses (arrows, I). Tau phosphorylated at serine 202 (labeled with CP13) and misfolded (residues 5-15 near 312-322, labelled with MC1) was also observed in PSDs (J). Images in A, G and large panels in J are maximum intensity projections of 10 serial sections. Scale bar represents 10 μm in A, G, J. B-D, H-I, and insets in J show three-dimensional reconstructions of a 2x2 micron region of interest in 5 consecutive serial 70nm sections. Data shown are median and interquartile ranges. Each dot represents the median of a single human subject (subject is the biological replicate/experimental unit n=6 per group). See also table S4.

MAIN TABLES AND LEGENDS

Table 1: Human subject characteristics

case	diagnosis	age	sex
1442	AD	80	f
1446	AD	84	m
1547	AD	77	m
1564	AD	90	m
AD5	AD	75	f
BBN24526	AD	79	m
HC	control	66	m
HC2	control	69	m
HC3	control	75	m
HC6	control	95	m
BBN28406	control	79	m
BBN19686	control	77	f

Table 2: Antibodies used in array tomography and histology studies. Host species were mouse (Ms), Rabbit (Rb), goat (Gt), and guinea pig (Gp).

Primary antibody	Species	Source (cat no)	Dilution	Secondary antibody
Mouse pathology study for amyloid burden and cortical and hippocampal volumes				
AW7	Rb	Dominic Walsh	1:5000	Donkey anti-rabbit Alexa594, Invitrogen
Mouse tau pathology study (independent stains)				
PHF1	Ms	P Davies	1:1000	Donkey anti-mouse Alexa594, Invitrogen
Alz50	Ms IgM	P Davies	1:1000	Donkey anti-mouse IgM Alexa594, Invitrogen

AT8	Ms	Thermo Fisher MN1020	1:1000	Donkey anti-mouse Alexa594, Invitrogen
Mouse study of gliosis burden				
Iba1	Gt	Abcam ab5076	1:500	Donkey anti-goat Alexa647, abcam
GFAP	Rb	DAKO Z0334	1:2000	Donkey anti-rabbit Alexa594, abcam
Mouse study of synaptic proteins inside microglia				
Synaptophysin	Ms	Abcam Ab8049	1:500	Donkey anti-mouse Alexa594, Invitrogen
Iba1	Gt	Abcam ab5076	1:500	Donkey anti-goat Alexa647, abcam
Mouse array tomography study of postsynaptic density and protein colocalisation				
PSD95	Rb	Cell signaling 3450P	1:50	Donkey anti-rabbit Alexa594, Invitrogen
Tau	Gt	R&D Systems	1:50	Donkey anti-goat Alexa647, Invitrogen
1C22	Ms	D Walsh	1:500	Donkey anti-mouse Alexa488, Invitrogen
Mouse array tomography study of presynaptic density and protein colocalisation				
synaptophysin	Ms	Abcam AB8049	1:50	Donkey anti-mouse Alexa594, Invitrogen
Tau	Gt	R&D Systems AF3494	1:50	Donkey anti-goat Alexa647, Invitrogen

AW7	Rb	D Walsh	1:500	Donkey anti-Rabbit Alexa488, Invitrogen
Human array tomography study of Tau13 synapse localization day 1				
synaptophysin	Ms	Abcam AB8049	1:50	Donkey anti-mouse Alexa488, Invitrogen
PSD95	Rb	Cell signaling 3450P	1:50	Donkey anti-rabbit Alexa594, Invitrogen
Human array tomography study of total tau synapse localization day 2				
Tau13	Ms	Covance MMS-520R		Donkey anti-mouse Alexa488, Invitrogen
AW7	Rb	D Walsh	1:500	Donkey anti-Rabbit Alexa594, Invitrogen

STAR METHODS

LEAD CONTACT AND MATERIALS AVAILABILTY

Further information and requests for resources and reagents should be directed to and will be fulfilled by the Lead Contact Prof Tara Spires-Jones (tara.spires-jones@ed.ac.uk). The new mouse line generated for this project was made using breeding of existing lines and in some cases material transfer agreements will be needed from the line originators before we can share lines.

EXPERIMENTAL MODEL AND SUBJECT DETAILS

Animals All animal experiments conformed to national and institutional guidelines including the Animals [Scientific Procedures Act] 1986 (UK), and the Council Directive 2010/63EU of the European Parliament and the Council of 22 September 2010 on the protection of animals used for scientific purposes, and had full Home Office ethical approval. Mice were bred in house and group housed in a 12h/12h light/dark cycle with ad libitum access to food and water. Both sexes of mice were used in all experiments (see table S1 for details of all mice used including sex, age, and weight information). Littermates were randomly assigned to experimental groups in experiments to reduce tau transgene expression and experimenters were blinded to genotype and treatment.

Human subjects Brain tissue samples were taken from superior temporal gyrus of 6 AD and 6 control subjects in the Edinburgh Sudden Death Brain Bank or the Massachusetts General Hospital Alzheimer's

Disease Research Centre Brain Bank. Characteristics of human subjects can be found in table 1 and synapse data in table S4. Average age was 81 for AD cases (range 75-90) and 77 for control cases (range 69-95). All AD cases were neuropathologically confirmed and were Braak stage V or VI. Control cases had no neurological phenotype. All human experiments were reviewed and approved by the Sudden Death Brain Bank ethics committee and the ACCORD medical research ethics committee (Academic and Clinical Central Office for Research and Development at the University of Edinburgh and National Health Service Lothian, ethical approval number 15-HV-016).

METHOD DETAILS

Generation of mouse line:

For the MAPTnull APP/PS1 rTg21221 (APP/PS1+Tau) model line, 4 genotypes were used to compare mice with (1) no transgene expression on a MAPTnull background (controls), (2) mice expressing human familial AD mutant APP and PS1 to generate Aß pathology (APP/PS1), (3) mice expressing 0N4R wild-type human tau (Tau), and (4) mice expressing both human tau and the APP/PS1 transgene (APP/PS1+Tau, **Fig. 1**). All mice were homozygous for deletion of mouse tau and heterozygous for the human wild-type tau transgene which is only expressed when the tetracycline transactivator transgene is also present. All experimental mice were F1 crosses from two feeder lines to maintain a controlled outbred background strain with consistent proportions of B6, B6C3, and FVB backgrounds. Parent strains used to generate the APP/PS1+Tau feeder lines were: (1) B6C3 APP/PS1 mice expressing human APP with the Swedish mutation and human presenilin 1 with an exon 9 deletion under the control of the Thy1 promoter (B6C3-Tg(APPsw,PSEN1dE9)85DboMmjax, Jax 34829) (Jankowsky et al., 2004); (2) MAPTnull mice which have the first exon of the *Mapt* gene replaced with EGFP (Tucker et al., 2001); (3) mice expressing the tetracycline transactivator under the control of the calcium calmodulin kinase 2 alpha promoter CK-tTA on the C57BL/6 backgrounds strain (B6.Cg-(Camk2a-tTA)1/MmayDboJ ,(Yasuda and Mayford, 2006)); (4) Tg21221 mice expressing human wild type tau under a dox-off tetracycline transactivator promotor (FVB-Tg(tetO-0N4R-MAPTwt)21221, (Hoover et al., 2010)). One feeder line was generated by crossing FVB.MAPTnull mice with the FVB.Tg21221 mice to generate FVB Tg21221 MAPTnull mice homozygous for both the Tg21221 transgene and the MAPT knockout. The other feeder line was generated by crossing B6C3 APP/PS1 mice with B6 MAPTnull mice to generate mice heterozygous for the APP/PS1 transgene and homozygous for the MAPT knockout. These two feeder lines were bred to generate F1 experimental animals. Human tau is only expressed when the tetracycline transactivator is also expressed and can be suppressed by feeding the mice doxycycline (Fig 1a). This consistent outbred background breeding scheme

keeps variability low while avoiding potential pitfalls of inbred strains such as sensory deficits during ageing, liver deficits, deletions such as loss of alpha-synuclein in some C57 strains, and other unknown recessive defects that may occur in inbred lines (Specht and Schoepfer, 2001, Cudalbu et al., 2013, Wong and Brown, 2006). Out of the 395 mice born during the generation and phenotyping of the APP/PS1+Tau line, as expected 100% were homozygous for endogenous tau knockout, 100% were heterozygous for the rTg21221 tau responder transgene, 53% were heterozygous for the APP/PS1 transgene (50% expected), 48% were heterozygous for the CK-tTA activator transgene (50% expected), and 23% had both the APP/PS1 and CK-tTA transgenes (25% expected). 48% of the mice were female. Thus, the transgenes were all inherited in the expected Mendelian ratios, indicating that no combination of genotypes was lethal (Chi squared value = 6.41, p= 0.093, df = 3 confirming Mendelian ratios). This is an important advantage of our consistent outbred breeding scheme as the same APP/PS1 transgene is lethal to about half of the mice on a congenic B6 background (Bennett et al., 2017). Genotyping of mice was carried out on ear notch samples using PCR primer sequences found in table S5.

One cohort of mice was aged and used for behavioural testing at 3, 6, and 9-10 months of age and sacrificed at 9-10 months of age for pathological characterization (see tables S1, S2, and S3 for all mouse data). Another cohort of mice was aged to 10-10.5 months of age, tested for baseline behaviour, then half of the mice were treated with 200ppm doxycycline in the chow for 4 months to reduce tau transgene expression and the others treated with control chow (vehicle). These mice underwent behavioural testing again at at 14-14.5 months of age then were sacrificed for pathological and molecular studies. Another cohort of littermates was aged to 6 months and sacrificed to look at onset of pathology.

As a negative control to be sure that any effects of tau expression were not an artefact of the CKtTA activator transgene, which is expressed in all mice that express tau by necessity, we examined B6.CKtTA mice on a mouse tau null background at 9 months of age for behavioural and pathological changes. As a positive control for tau staining rTg4510 brain sections from 3 mice were used for tau immunohistochemistry (Santacruz et al., 2005, Spires et al., 2006).

Behavioural testing

Group sizes for behavioural studies in the APP/PS1+Tau line can be found in figure legends and table S1. We used distance travelled in an open field to determine whether mice had a hyperactivity phenotype as

has been used by multiple groups previously as a proxy for hyperactivity in AD model mice (see for example Blackmore et al., 2017, Yetman et al., 2016). Animals were tested for open field behaviour in a square box (40 x 40 x 60 cm) composed of dark opaque walls with approximately 2.5cm of corn cob bedding on the floor of the arena. Animals were recorded using an overhead camera and the video signal fed into Blackmagic Media Express computer software which captured the animals' movements. Each day animals were brought into the testing room in their home cage upon the end of the 12 hr dark cycle and allowed to settle for 1 hour. For habituation, animals were exposed to the open field for 3 consecutive days. On day 1, animals were introduced to the centre of the arena along with cage mates for 20 minutes. For days 2-4, individual animals were placed facing a corner of the arena, which was assigned using a random generator. For each experimental group, the order in which animals were placed in the arena was randomly assigned using a random sequence generator. On day 4, behaviour in the open field was recorded for 10 minutes using an overhead camera and movements captured with Blackmagic Media Express software. idTracker software and MATLAB were used to analyse mouse behaviour. The total distance travelled, distance travelled in the outer segment (40 x 40 – inner segment), distance travelled in the inner segment (20 x 20), percentage of time spent in the outer segment and percentage of time spent in the inner segment, were calculated and analysed in SPSS and Prism7.

In order to ensure that the hyperactivity observed at 14.5 months of age is not a consequence of baseline performance prior to treatment, 10.5 month old mice were assessed for baseline performance in the open field according to the treatment group to which they would be assigned. A significant effect of genotype was observed ($p<0.0001$), however there was no difference in open field behaviour in the cohorts destined for doxycycline or vehicle treatment within the same genotype (2-way ANOVA effect of treatment $F(1,164)=0$, $p>0.99999$). This suggests the increase in total distance travelled in 14.5 month old vehicle-treated APP/PS1+Tau mice and reversal with doxycycline is not due to baseline increased activity in this group at 10.5 months of age.

Measuring pathology

Mice were sacrificed by terminal anaesthesia and perfused with PBS. Brains were dissected and one hemisphere fixed for 48 hours in 4% paraformaldehyde. Samples of entorhinal cortex from the other hemisphere were saved for array tomography as detailed below and the rest of the hemisphere was

frozen for biochemical analyses. The fixed hemisphere was cryoprotected in 15% glycerol and sectioned into 50 micron coronal sections through the entire hemisphere with a sliding microtome (Leica SM2010R sliding microtome). To quantify amyloid pathology, every 20th section was stained with a pan-Aß antibody and counterstained with 0.05% Thioflavine S in 50% ethanol to label plaque fibrils and any neurofibrillary tangles (antibody details are found in table 2). Tile scan images of each entire section were obtained with a 10x objective on a Zeiss Axioimager microscope. Images were analysed using ImageJ. The cortex and hippocampus on each section were outlined, regions of interest defined, and the area calculated. Cortical and hippocampal volumes were estimated by multiplying the area on each section by 1000 (distance between sections), summing these values for all sections, and multiplying by 2 to estimate total volume as we only measured one hemisphere. Each channel of amyloid staining was manually thresholded in ImageJ by an experimenter blinded to genotype. The ImageJ analyze particles function was used to calculate the percent area of cortex and hippocampus occupied by staining and the number and average size of individual plaques. To calculate the burden of oligomeric halos surrounding plaques, the thresholded Thioflavin S image was subtracted from the thresholded pan-Aß image and plaque burden, number, and size were analysed as above.

Series of every 10th section were also stained with pathological tau antibodies to look for neurofibrillary tangles and neuropil threads as detailed in table 2. Stained sections were examined using a Zeiss AxioImager Z2 microscope and images acquired with a CoolSnap digital camera. For tau stains, rTg4510 mouse brain sections containing neurofibrillary pathology were used as positive controls.

To measure gliosis burden, free floating coronal sections were stained for microglia (Iba1), astrocytes (GFAP), and fibrillary plaques (Thioflavine S), with citrate buffer pre-treatment (95^{o}C for 20 minutes, see table 2 for antibody details). Three coronal sections were stained per mouse at approximately 0.75mm, -2.0mm, and -3.75mm from Bregma. Tile scans were obtained at 10x magnification using a ZEISS Imager.Z2 microscope and images were thresholded on ImageJ for cortical burden quantification. For all immunostains, no primary conditions were used as negative controls.

To examine synaptic proteins within microglia, 2 coronal sections per mouse (Bregma -1.0 and -3.0, n=5 mice per group) were stained for microglia (Iba1), synaptophysin (SY38), DAPI, and fibrillar plaques (Thioflavine S 0.05% in 50% ethanol). Citrate buffer pre-treatment was used for antigen retrieval (95^{o}C for 20 minutes, see table 2 for antibody details). Confocal image stacks were acquired on a Leica TCS SP8 confocal with z-step of 1 micron. Z-stack reconstructions were performed in ImageJ and Imaris to confirm

synaptic proteins within Iba1 positive cells.

RNA analyses

Total RNA was extracted from the frontal cortex using the Lipid Tissue Mini Kit (Qiagen). RNA quantity and quality was assessed using a Bioanalyzer 2100 (Agilent Technologies). All samples had RIN values > 7. To generate RNA-seq data, barcoded RNA-seq libraries were prepared by Edinburgh Genomics using the Illumina TruSeq stranded mRNA-seq kit, according to the manufacturer's protocol (Illumina). The libraries were pooled and sequenced using an Illumina Novaseq 6000. RNA-sequencing was performed to a depth of ~60 million 50bp paired-end reads per sample. Reads were mapped to the mouse primary genome assembly (GRCm38) contained in Ensembl release 92 (Zerbino et al., 2018). Read alignment was performed with STAR (Dobin et al., 2013), version 2.5.3a, and tables of per-gene read counts were generated from the mapped reads with featureCounts (Liao et al., 2014), version 1.5.2. Differential expression analysis was then performed using DESeq2 (R package version 1.18.1) (Love et al., 2014). Gene Ontology enrichment analysis was performed with topGO [5] (R package version 2.30.1), and pathway analyses were performed with Ingenuity Pathway Analysis software (Krämer et al., 2013). An adjusted p value cut-off of <0.05 was set to identify molecules whose expression was differentially regulated.

For qRT-PCR, cDNA was synthesised using the SuperScript VILO cDNA synthesis kit (ThermoFisher) and the following PCR settings used: 10 minutes at 25°C, 60 minutes at 42°C and 5 minutes at 85°C. qPCRs were run on a Stratagene Mx3000P QPCR System (Agilent Technologies) using SYBR Green MasterRox (Roche) with 6 ng of cDNA per well of a 96-well plate, using the following programme: 10 min at 95 °C, 40 cycles of 30 s at 95 °C, 40 s at 60 °C and 30 s at 72 °C, with a subsequent cycle of 1 min at 95 °C and 30 s at 55 °C ramping up to 95 °C over 30 s (to measure the dissociation curve). Primers used are found in table S5.

Array Tomography

Fresh brain tissue samples were collected from 14.5 month old mice and human subjects as outlined previously (Koffie et al., 2009, Kay et al., 2013). Small tissue blocks containing cortex were fixed in 4% paraformaldehyde and 2.5% sucrose in 20 mM phosphate buffered saline pH 7.4 (PBS) for 3 hours. Samples were then dehydrated through ascending cold graded ethanol and embedded into LR White resin (EMS) which was allowed to polymerise overnight at 53 °C. Resin embedded tissue blocks were cut into

array ribbons of 70 nm thick sections using an ultracut microtome (Leica) equipped with a Jumbo Histo Diamond Knife (Diatome, Hatfield, PA) and collected onto gelatin coated coverslips.

For pathological protein colocalisation with postsynapses, array ribbons were immunostained with primary antibodies against post synapses (PSD95), oligomeric Aβ (1C22) and total tau (pan-tau). For pathological protein colocalisation with pre-synapses, array ribbons were immunostained with primary antibodies against synaptic vesicle protein synaptophysin, Aβ (AW7) and total tau (pan-tau) (Table 2). Sections were counterstained with 0.01 mg/mL 4'-6-diamidino-2-phenylindole (DAPI). In each experiment, a short extra ribbon was used as a no primary negative control. Images were obtained on serial sections using a Zeiss axio Imager Z2 epifluorescent microscope with a 10x objective for tile scans and 63x 1.4NA Plan Apochromat objective for high resolution images. Images were acquired with a CoolSnap digital camera and AxioImager software with array tomography macros (Carl Zeiss, Ltd, Cambridge UK).

Human brain array tomography ribbons were stained with combinations of synaptic antibodies, tau antibodies and AW7 to label amyloid beta as described in the Figs and table 2. For two-day stains, antibodies applied for the first imaging day were stripped by incubation in aqueous 0.02% SDS and 0.8% sodium hydroxide solution for 20 minutes. Stripped ribbons were rinsed in water and re-probed with another set of primary then secondary antibodies.

Images from each set of serial sections were converted into image stacks and aligned using the Image J plug-in, MultiStackReg (courtesy of Brad Busse and P. Thevenaz, Stanford University) (Thevenaz et al., 1998). Regions of interest within the cortical neuropil were chosen (10 μm^2) and their proximity to plaque edges recorded (<20 μm from a plaque edge considered "near" plaques and >20 μm from a plaque edge considered "far" from plaques). Image stacks were then binarised using thresholding algorithms in ImageJ. For synaptic staining, images stacks were binarised using an ImageJ script that combines different thresholding algorithms in order to select both high and low intensity synapses in an automated and unbiased manner. To calculate the synaptic density, thresholded images were processed and analysed in MATLAB to remove background noise (objects present in only a single section were removed). To examine pathological protein presence at the synapse, thresholded images were processed and analysed in MATLAB to remove background noise and to calculate the colocalisation of total tau and oligomeric Aβ

with post synapses individually and in combination (a minimum of 50% of the synapse volume had to overlap with tau and/or 1C22 to qualify as positive for that stain).

QUANTIFICATION AND STATISTICAL ANALYSIS

All experiments were carried out by a person blind to genotype and treatment of the mice and blind to diagnosis for human studies. For each experimental variable, a percentage, mean or median was calculated for each subject (experimental unit was the mouse or human case). Groups of mice or people were compared with parametric or non-parametric tests as appropriate based on the normality of the datasets as assessed by Shapiro-Wilks tests. Statistical tests were carried out in SPSS and Prism7. The number of subjects and statistical tests used for each experiment are indicated in the results, Fig legends, and data analysed is found in tables S1 and S2 (mouse) and S4 (human).

DATA AND SOFTWARE AVAILABILITY

Spreadsheets of all data used in this study are included as tables S1-S4. The RNA-seq data generated during this study are available at the European Bioinformatics Institute depository (https://www.ebi.ac.uk/arrayexpress/experiments/E-MTAB-7856/). Custom imageJ and MATLAB macros used for image analysis are freely available on the University of Edinburgh Data Sharing repository (https://doi.org/10.7488/ds/2592).

Supplemental files:

table S1 – individual mouse pathology data. Related to figures 1-4.

table S2 – mouse RNAseq results. Related to figures 2, 3.

table S3 – canonical pathways in Ingenuity Pathway Analysis of mouse RNAseq data, related to figures 2, 3.

table S4 – individual human array tomography data. Related to figure 5.

table S5 – oligonucleotides, related to STAR methods

References

BARRY, A. E., KLYUBIN, I., MC DONALD, J. M., MABLY, A. J., FARRELL, M. A., SCOTT, M., WALSH, D. M. & ROWAN, M. J. 2011. Alzheimer's disease brain-derived amyloid-beta-mediated inhibition of LTP in vivo is prevented by immunotargeting cellular prion protein. *J Neurosci,* 31**,** 7259-63.

BENNETT, R. E., BRYANT, A., HU, M., ROBBINS, A. B., HOPP, S. C. & HYMAN, B. T. 2018. Partial reduction of microglia does not affect tau pathology in aged mice. *Journal of Neuroinflammation,* 15**,** 311.

BENNETT, R. E., DEVOS, S. L., DUJARDIN, S., CORJUC, B., GOR, R., GONZALEZ, J., ROE, A. D., FROSCH, M. P., PITSTICK, R., CARLSON, G. A. & HYMAN, B. T. 2017. Enhanced Tau Aggregation in the Presence of Amyloid beta. *Am J Pathol,* 187**,** 1601-1612.

BLACKMORE, T., MEFTAH, S., MURRAY, T. K., CRAIG, P. J., BLOCKEEL, A., PHILLIPS, K., EASTWOOD, B., O'NEILL, M. J., MARSTON, H., AHMED, Z., GILMOUR, G. & GASTAMBIDE, F. 2017. Tracking progressive pathological and functional decline in the rTg4510 mouse model of tauopathy. *Alzheimers Res Ther,* 9**,** 77.

BUSCHE, M. A., WEGMANN, S., DUJARDIN, S., COMMINS, C., SCHIANTARELLI, J., KLICKSTEIN, N., KAMATH, T. V., CARLSON, G. A., NELKEN, I. & HYMAN, B. T. 2019. Tau impairs neural circuits, dominating amyloid-β effects, in Alzheimer models in vivo. *Nature Neuroscience,* 22**,** 57-64.

CRIMINS, J. L., POOLER, A., POLYDORO, M., LUEBKE, J. I. & SPIRES-JONES, T. L. 2013. The intersection of amyloid beta and tau in glutamatergic synaptic dysfunction and collapse in Alzheimer's disease. *Ageing Res Rev*.

CUDALBU, C., MCLIN, V. A., LEI, H., DUARTE, J. M., ROUGEMONT, A. L., OLDANI, G., TERRAZ, S., TOSO, C. & GRUETTER, R. 2013. The C57BL/6J mouse exhibits sporadic congenital portosystemic shunts. *PLoS One,* 8**,** e69782.

DE STROOPER, B. & KARRAN, E. 2016. The Cellular Phase of Alzheimer's Disease. *Cell,* 164**,** 603-615.

DEJANOVIC, B., HUNTLEY, M. A., DE MAZIERE, A., MEILANDT, W. J., WU, T., SRINIVASAN, K., JIANG, Z., GANDHAM, V., FRIEDMAN, B. A., NGU, H., FOREMAN, O., CARANO, R. A. D., CHIH, B., KLUMPERMAN, J., BAKALARSKI, C., HANSON, J. E. & SHENG, M. 2018. Changes in the Synaptic Proteome in Tauopathy and Rescue of Tau-Induced Synapse Loss by C1q Antibodies. *Neuron,* 100**,** 1322-1336 e7.

DEVOS, S. L., CORJUC, B. T., COMMINS, C., DUJARDIN, S., BANNON, R. N., CORJUC, D., MOORE, B. D., BENNETT, R. E., JORFI, M., GONZALES, J. A., DOOLEY, P. M., ROE, A. D., PITSTICK, R., IRIMIA, D., FROSCH, M. P., CARLSON, G. A. & HYMAN, B. T. 2018a. Tau reduction in the presence of amyloid-β prevents tau pathology and neuronal death in vivo. *Brain,* 141**,** 2194-2212.

DEVOS, S. L., CORJUC, B. T., OAKLEY, D. H., NOBUHARA, C. K., BANNON, R. N., CHASE, A., COMMINS, C., GONZALEZ, J. A., DOOLEY, P. M., FROSCH, M. P. & HYMAN, B. T. 2018b. Synaptic Tau Seeding Precedes Tau Pathology in Human Alzheimer's Disease Brain. *Frontiers in Neuroscience,* 12.

DOBIN, A., DAVIS, C. A., SCHLESINGER, F., DRENKOW, J., ZALESKI, C., JHA, S., BATUT, P., CHAISSON, M. & GINGERAS, T. R. 2013. STAR: ultrafast universal RNA-seq aligner. *Bioinformatics,* 29**,** 15-21.

FOX, L. M., WILLIAM, C. M., ADAMOWICZ, D. H., PITSTICK, R., CARLSON, G. A., SPIRES-JONES, T. L. & HYMAN, B. T. 2011. Soluble tau species, not neurofibrillary aggregates, disrupt neural system integration in a tau transgenic model. *J Neuropathol Exp Neurol,* 70**,** 588-95.

FU, H., RODRIGUEZ, G. A., HERMAN, M., EMRANI, S., NAHMANI, E., BARRETT, G., FIGUEROA, H. Y., GOLDBERG, E., HUSSAINI, S. A. & DUFF, K. E. 2017. Tau Pathology Induces Excitatory Neuron Loss, Grid Cell Dysfunction, and Spatial Memory Deficits Reminiscent of Early Alzheimer's Disease. *Neuron,* 93**,** 533-541 e5.

GRUNDMAN, M., MORGAN, R., LICKLITER, J. D., SCHNEIDER, L. S., DEKOSKY, S., IZZO, N. J., GUTTENDORF, R., HIGGIN, M., PRIBYL, J., MOZZONI, K., SAFFERSTEIN, H. & CATALANO, S. M. 2019. A phase 1 clinical trial of the sigma-2 receptor complex allosteric antagonist CT1812, a novel therapeutic candidate for Alzheimer's disease. *Alzheimers Dement (N Y),* 5**,** 20-26.

HAAS, L. T. & STRITTMATTER, S. M. 2016. Oligomers of Amyloid beta Prevent Physiological Activation of the Cellular Prion Protein-Metabotropic Glutamate Receptor 5 Complex by Glutamate in Alzheimer Disease. *J Biol Chem,* 291**,** 17112-21.

HARDY, J. A. & HIGGINS, G. A. 1992. Alzheimer's disease: the amyloid cascade hypothesis. *Science,* 256**,** 184-5.

HENSTRIDGE, C. M., HYMAN, B. T. & SPIRES-JONES, T. L. 2019. Beyond the neuron–cellular interactions early in Alzheimer disease pathogenesis. *Nature Reviews Neuroscience,* 20**,** 94-108.

HONG, S., BEJA-GLASSER, V. F., NFONOYIM, B. M., FROUIN, A., LI, S., RAMAKRISHNAN, S., MERRY, K. M., SHI, Q., ROSENTHAL, A., BARRES, B. A., LEMERE, C. A., SELKOE, D. J. & STEVENS, B. 2016. Complement and microglia mediate early synapse loss in Alzheimer mouse models. *Science*.

HOOVER, B. R., REED, M. N., SU, J., PENROD, R. D., KOTILINEK, L. A., GRANT, M. K., PITSTICK, R., CARLSON, G. A., LANIER, L. M., YUAN, L.-L., ASHE, K. H. & LIAO, D. 2010. Tau Mislocalization to Dendritic Spines Mediates Synaptic Dysfunction Independently of Neurodegeneration. *Neuron,* 68**,** 1067-1081.

HU, N. W., CORBETT, G. T., MOORE, S., KLYUBIN, I., O'MALLEY, T. T., WALSH, D. M., LIVESEY, F. J. & ROWAN, M. J. 2018. Extracellular Forms of Abeta and Tau from iPSC Models of Alzheimer's Disease Disrupt Synaptic Plasticity. *Cell Rep,* 23**,** 1932-1938.

HU, N. W., NICOLL, A. J., ZHANG, D., MABLY, A. J., O'MALLEY, T., PURRO, S. A., TERRY, C., COLLINGE, J., WALSH, D. M. & ROWAN, M. J. 2014. mGlu5 receptors and cellular prion protein mediate amyloid-beta-facilitated synaptic long-term depression in vivo. *Nat Commun,* 5**,** 3374.

HUDRY, E., WU, H. Y., ARBEL-ORNATH, M., HASHIMOTO, T., MATSOUAKA, R., FAN, Z., SPIRES-JONES, T. L., BETENSKY, R. A., BACSKAI, B. J. & HYMAN, B. T. 2012. Inhibition of the NFAT pathway alleviates amyloid beta neurotoxicity in a mouse model of Alzheimer's disease. *J Neurosci,* 32**,** 3176-92.

HYMAN, B. T. 2011. Amyloid-dependent and amyloid-independent stages of Alzheimer disease. *Arch Neurol,* 68**,** 1062-4.

ITTNER, L. M., KE, Y. D., DELERUE, F., BI, M., GLADBACH, A., VAN EERSEL, J., WOLFING, H., CHIENG, B. C., CHRISTIE, M. J., NAPIER, I. A., ECKERT, A., STAUFENBIEL, M., HARDEMAN, E. & GOTZ, J. 2010. Dendritic function of tau mediates amyloid-beta toxicity in Alzheimer's disease mouse models. *Cell,* 142**,** 387-97.

IZZO, N. J., STANISZEWSKI, A., TO, L., FA, M., TEICH, A. F., SAEED, F., WOSTEIN, H., WALKO, T., 3RD, VASWANI, A., WARDIUS, M., SYED, Z., RAVENSCROFT, J., MOZZONI, K., SILKY, C., REHAK, C., YURKO, R., FINN, P., LOOK, G., RISHTON, G., SAFFERSTEIN, H., MILLER, M., JOHANSON, C., STOPA, E., WINDISCH, M., HUTTER-PAIER, B., SHAMLOO, M., ARANCIO, O., LEVINE, H., 3RD & CATALANO, S. M. 2014. Alzheimer's therapeutics targeting amyloid beta 1-42 oligomers I: Abeta 42 oligomer binding to specific neuronal receptors is displaced by drug candidates that improve cognitive deficits. *PLoS One,* 9**,** e111898.

JACKSON, R. J., ROSE, J., TULLOCH, J., HENSTRIDGE, C., SMITH, C. & SPIRES-JONES, T. L. 2019. Clusterin accumulates in synapses in Alzheimer's disease and is increased in apolipoprotein E4 carriers. *Brain Communications,* 1.

JACKSON, R. J., RUDINSKIY, N., HERRMANN, A. G., CROFT, S., KIM, J. M., PETROVA, V., RAMOS-RODRIGUEZ, J. J., PITSTICK, R., WEGMANN, S., GARCIA-ALLOZA, M., CARLSON, G. A., HYMAN, B. T. & SPIRES-JONES, T. L. 2016. Human tau increases amyloid beta plaque size but not amyloid beta-mediated synapse loss in a novel mouse model of Alzheimer's disease. *Eur J Neurosci,* 44**,** 3056-3066.

JANKOWSKY, J. L., FADALE, D. J., ANDERSON, J., XU, G. M., GONZALES, V., JENKINS, N. A., COPELAND, N. G., LEE, M. K., YOUNKIN, L. H., WAGNER, S. L., YOUNKIN, S. G. & BORCHELT, D. R. 2004. Mutant presenilins specifically elevate the levels of the 42 residue beta-amyloid peptide in vivo: evidence for augmentation of a 42-specific gamma secretase. *Hum Mol Genet,* 13**,** 159-70.

JAROSZ-GRIFFITHS, H. H., NOBLE, E., RUSHWORTH, J. V. & HOOPER, N. M. 2016. Amyloid-beta Receptors: The Good, the Bad, and the Prion Protein. *J Biol Chem,* 291**,** 3174-83.

JAY, T. R., HIRSCH, A. M., BROIHIER, M. L., MILLER, C. M., NEILSON, L. E., RANSOHOFF, R. M., LAMB, B. T. & LANDRETH, G. E. 2017. Disease Progression-Dependent Effects of TREM2 Deficiency in a Mouse Model of Alzheimer's Disease. *J Neurosci,* 37**,** 637-647.

KAY, K. R., SMITH, C., WRIGHT, A. K., SERRANO-POZO, A., POOLER, A. M., KOFFIE, R., BASTIN, M. E., BAK, T. H., ABRAHAMS, S., KOPEIKINA, K. J., MCGUONE, D., FROSCH, M. P., GILLINGWATER, T. H., HYMAN, B. T. & SPIRES-JONES, T. L. 2013. Studying synapses in human brain with array tomography and electron microscopy. *Nat Protoc,* 8**,** 1366-80.

KLEIN, W. 2013. Synaptotoxic amyloid-β oligomers: a molecular basis for the cause, diagnosis, and treatment of Alzheimer's disease? *Journal of Alzheimer's disease : JAD,* 33 Suppl 1**,** 65.

KOFFIE, R. M., HASHIMOTO, T., TAI, H. C., KAY, K. R., SERRANO-POZO, A., JOYNER, D., HOU, S., KOPEIKINA, K. J., FROSCH, M. P., LEE, V. M., HOLTZMAN, D. M., HYMAN, B. T. & SPIRES-JONES, T.

L. 2012. Apolipoprotein E4 effects in Alzheimer's disease are mediated by synaptotoxic oligomeric amyloid-beta. *Brain,* 135**,** 2155-68.

KOFFIE, R. M., MEYER-LUEHMANN, M., HASHIMOTO, T., ADAMS, K. W., MIELKE, M. L., GARCIA-ALLOZA, M., MICHEVA, K. D., SMITH, S. J., KIM, M. L., LEE, V. M., HYMAN, B. T. & SPIRES-JONES, T. L. 2009. Oligomeric amyloid beta associates with postsynaptic densities and correlates with excitatory synapse loss near senile plaques. *Proc Natl Acad Sci U S A,* 106**,** 4012-7.

KOPEIKINA, K. J., HYMAN, B. T. & SPIRES-JONES, T. L. 2012. Soluble forms of tau are toxic in Alzheimer's disease. *Transl Neurosci,* 3**,** 223-233.

KRÄMER, A., POLLARD, J., JR, GREEN, J. & TUGENDREICH, S. 2013. Causal analysis approaches in Ingenuity Pathway Analysis. *Bioinformatics,* 30**,** 523-530.

KUCHIBHOTLA, K. V., GOLDMAN, S. T., LATTARULO, C. R., WU, H. Y., HYMAN, B. T. & BACSKAI, B. J. 2008. Abeta plaques lead to aberrant regulation of calcium homeostasis in vivo resulting in structural and functional disruption of neuronal networks. *Neuron,* 59**,** 214-25.

LI, S., HONG, S., SHEPARDSON, N. E., WALSH, D. M., SHANKAR, G. M. & SELKOE, D. 2009. Soluble oligomers of amyloid Beta protein facilitate hippocampal long-term depression by disrupting neuronal glutamate uptake. *Neuron,* 62**,** 788-801.

LIAO, Y., SMYTH, G. K. & SHI, W. 2014. featureCounts: an efficient general purpose program for assigning sequence reads to genomic features. *Bioinformatics,* 30**,** 923-30.

LITVINCHUK, A., WAN, Y. W., SWARTZLANDER, D. B., CHEN, F., COLE, A., PROPSON, N. E., WANG, Q., ZHANG, B., LIU, Z. & ZHENG, H. 2018. Complement C3aR Inactivation Attenuates Tau Pathology and Reverses an Immune Network Deregulated in Tauopathy Models and Alzheimer's Disease. *Neuron,* 100**,** 1337-1353 e5.

LOVE, M. I., HUBER, W. & ANDERS, S. 2014. Moderated estimation of fold change and dispersion for RNA-seq data with DESeq2. *Genome Biol,* 15**,** 550.

LOVESTONE, S., HYE, A. & DIXIT, A. 2014. Clusterin as an early medator of Ab-induced disease processes: evidence from man *Alzheimer's & Dementia,* 10**,** 161.

MARZO, A., GALLI, S., LOPES, D., MCLEOD, F., PODPOLNY, M., SEGOVIA-ROLDAN, M., CIANI, L., PURRO, S., CACUCCI, F., GIBB, A. & SALINAS, P. C. 2016. Reversal of Synapse Degeneration by Restoring Wnt Signaling in the Adult Hippocampus. *Curr Biol,* 26**,** 2551-2561.

MATARIN, M., SALIH, D. A., YASVOINA, M., CUMMINGS, D. M., GUELFI, S., LIU, W., NAHABOO SOLIM, M. A., MOENS, T. G., PAUBLETE, R. M., ALI, S. S., PERONA, M., DESAI, R., SMITH, K. J., LATCHAM, J., FULLEYLOVE, M., RICHARDSON, J. C., HARDY, J. & EDWARDS, F. A. 2015. A genome-wide gene-expression analysis and database in transgenic mice during development of amyloid or tau pathology. *Cell Rep,* 10**,** 633-44.

MATTSON, M. P., CHENG, B., DAVIS, D., BRYANT, K., LIEBERBURG, I. & RYDEL, R. E. 1992. beta-Amyloid peptides destabilize calcium homeostasis and render human cortical neurons vulnerable to excitotoxicity. *J Neurosci,* 12**,** 376-89.

MCINNES, J., WIERDA, K., SNELLINX, A., BOUNTI, L., WANG, Y. C., STANCU, I. C., APOSTOLO, N., GEVAERT, K., DEWACHTER, I., SPIRES-JONES, T. L., DE STROOPER, B., DE WIT, J., ZHOU, L. & VERSTREKEN, P. 2018. Synaptogyrin-3 Mediates Presynaptic Dysfunction Induced by Tau. *Neuron,* 97**,** 823-835 e8.

MENKES-CASPI, N., YAMIN, H. G., KELLNER, V., SPIRES-JONES, T. L., COHEN, D. & STERN, E. A. 2015. Pathological tau disrupts ongoing network activity. *Neuron,* 85**,** 959-66.

MUCKE, L. & SELKOE, D. 2012. Neurotoxicity of amyloid β-protein: synaptic and network dysfunction. *Cold Spring Harb Perspect Med,* 2.

OVSEPIAN, S. V., O'LEARY, V. B., ZABORSZKY, L., NTZIACHRISTOS, V. & DOLLY, J. O. 2018. Synaptic vesicle cycle and amyloid beta: Biting the hand that feeds. *Alzheimers Dement,* 14**,** 502-513.

PRINCE, M., ANDERS, W., GUERCGET, M., ALI, G.-C., WU, Y.-T. & PRINA, M. 2015. World Alzheiemr Report 2015 - the Global Impact of Dementia. Alzheimer's Disease International.

PURRO, S. A., DICKINS, E. M. & SALINAS, P. C. 2012. The secreted Wnt antagonist Dickkopf-1 is required for amyloid β-mediated synaptic loss. *The Journal of Neuroscience*.

ROBERSON, E. D., HALABISKY, B., YOO, J. W., YAO, J., CHIN, J., YAN, F., WU, T., HAMTO, P., DEVIDZE, N., YU, G. Q., PALOP, J. J., NOEBELS, J. L. & MUCKE, L. 2011. Amyloid-beta/Fyn-induced synaptic, network, and cognitive impairments depend on tau levels in multiple mouse models of Alzheimer's disease. *J Neurosci,* 31**,** 700-11.

ROBERSON, E. D., SCEARCE-LEVIE, K., PALOP, J. J., YAN, F., CHENG, I. H., WU, T., GERSTEIN, H., YU, G. Q. & MUCKE, L. 2007. Reducing endogenous tau ameliorates amyloid beta-induced deficits in an Alzheimer's disease mouse model. *Science,* 316**,** 750-4.

SANTACRUZ, K., LEWIS, J., SPIRES, T., PAULSON, J., KOTILINEK, L., INGELSSON, M., GUIMARAES, A., DETURE, M., RAMSDEN, M., MCGOWAN, E., FORSTER, C., YUE, M., ORNE, J., JANUS, C., MARIASH, A., KUSKOWSKI, M., HYMAN, B., HUTTON, M. & ASHE, K. H. 2005. Tau suppression in a neurodegenerative mouse model improves memory function. *Science,* 309**,** 476-81.

SASAGURI, H., NILSSON, P., HASHIMOTO, S., NAGATA, K., SAITO, T., DE STROOPER, B., HARDY, J., VASSAR, R., WINBLAD, B. & SAIDO, T. C. 2017. APP mouse models for Alzheimer's disease preclinical studies. *EMBO J,* 36**,** 2473-2487.

SELLERS, K. J., ELLIOTT, C., JACKSON, J., GHOSH, A., RIBE, E., ROJO, A. I., JAROSZ-GRIFFITHS, H. H., WATSON, I. A., XIA, W., SEMENOV, M., MORIN, P., HOOPER, N. M., PORTER, R., PRESTON, J., AL-SHAWI, R., BAILLIE, G., LOVESTONE, S., CUADRADO, A., HARTE, M., SIMONS, P., SRIVASTAVA, D. P. & KILLICK, R. 2018. Amyloid beta synaptotoxicity is Wnt-PCP dependent and blocked by fasudil. *Alzheimers Dement,* 14**,** 306-317.

SHI, Q., CHOWDHURY, S., MA, R., LE, K. X., HONG, S., CALDARONE, B. J., STEVENS, B. & LEMERE, C. A. 2017. Complement C3 deficiency protects against neurodegeneration in aged plaque-rich APP/PS1 mice. *Sci Transl Med,* 9.

SHIPTON, O., LEITZ, J., DWORZAK, J., ACTON, C., TUNBRIDGE, E., DENK, F., DAWSON, H., VITEK, M., WADE-MARTINS, R., PAULSEN, O. & VARGAS-CABALLERO, M. 2011. Tau protein is required for amyloid {beta}-induced impairment of hippocampal long-term potentiation. *The Journal of neuroscience : the official journal of the Society for Neuroscience,* 31**,** 1688-1692.

SMALL, S. A. & DUFF, K. 2008. Linking Aβ and tau in late-onset Alzheimer's disease: a dual pathway hypothesis. *Neuron*.

SPECHT, C. G. & SCHOEPFER, R. 2001. Deletion of the alpha-synuclein locus in a subpopulation of C57BL/6J inbred mice. *BMC Neurosci,* 2**,** 11.

SPIRES, T. L., MEYER-LUEHMANN, M., STERN, E. A., MCLEAN, P. J., SKOCH, J., NGUYEN, P. T., BACSKAI, B. J. & HYMAN, B. T. 2005. Dendritic spine abnormalities in amyloid precursor protein transgenic mice demonstrated by gene transfer and intravital multiphoton microscopy. *J Neurosci,* 25**,** 7278-87.

SPIRES, T. L., ORNE, J. D., SANTACRUZ, K., PITSTICK, R., CARLSON, G. A., ASHE, K. H. & HYMAN, B. T. 2006. Region-specific dissociation of neuronal loss and neurofibrillary pathology in a mouse model of tauopathy. *Am J Pathol,* 168**,** 1598-607.

SPIRES-JONES, T. L., ATTEMS, J. & THAL, D. R. 2017. Interactions of pathological proteins in neurodegenerative diseases. *Acta Neuropathol,* 134**,** 187-205.

SPIRES-JONES, T. L. & HYMAN, B. T. 2014. The intersection of amyloid beta and tau at synapses in Alzheimer's disease. *Neuron,* 82**,** 756-71.

SPIRES-JONES, T. L., MEYER-LUEHMANN, M., OSETEK, J. D., JONES, P. B., STERN, E. A., BACSKAI, B. J. & HYMAN, B. T. 2007. Impaired spine stability underlies plaque-related spine loss in an Alzheimer's disease mouse model. *Am J Pathol,* 171**,** 1304-11.

SPIRES-JONES, T. L., MIELKE, M. L., ROZKALNE, A., MEYER-LUEHMANN, M., DE CALIGNON, A., BACSKAI, B. J., SCHENK, D. & HYMAN, B. T. 2009. Passive immunotherapy rapidly increases structural plasticity in a mouse model of Alzheimer disease. *Neurobiol Dis,* 33**,** 213-20.

TERRY, R. D., MASLIAH, E., SALMON, D. P., BUTTERS, N., DETERESA, R., HILL, R., HANSEN, L. A. & KATZMAN, R. 1991. Physical basis of cognitive alterations in Alzheimer's disease: synapse loss is the major correlate of cognitive impairment. *Ann Neurol,* 30**,** 572-80.

THEVENAZ, P., RUTTIMANN, U. E. & UNSER, M. 1998. A pyramid approach to subpixel registration based on intensity. *IEEE Trans Image Process,* 7**,** 27-41.

TUCKER, K. L., MEYER, M. & BARDE, Y. A. 2001. Neurotrophins are required for nerve growth during development. *Nat Neurosci,* 4**,** 29-37.

UM, J. W., KAUFMAN, A. C., KOSTYLEV, M., HEISS, J. K., STAGI, M., TAKAHASHI, H., KERRISK, M. E., VORTMEYER, A., WISNIEWSKI, T., KOLESKE, A. J., GUNTHER, E. C., NYGAARD, H. B. & STRITTMATTER, S. M. 2013. Metabotropic glutamate receptor 5 is a coreceptor for Alzheimer abeta oligomer bound to cellular prion protein. *Neuron,* 79**,** 887-902.

UM, J. W., NYGAARD, H. B., HEISS, J. K., KOSTYLEV, M. A., STAGI, M., VORTMEYER, A., WISNIEWSKI, T., GUNTHER, E. C. & STRITTMATTER, S. M. 2012. Alzheimer amyloid-beta oligomer bound to postsynaptic prion protein activates Fyn to impair neurons. *Nat Neurosci,* 15**,** 1227-35.

VARGAS-CABALLERO, M., DENK, F., WOBST, H. J., ARCH, E., PEGASIOU, C. M., OLIVER, P. L., SHIPTON, O. A., PAULSEN, O. & WADE-MARTINS, R. 2017. Wild-Type, but Not Mutant N296H, Human Tau Restores Abeta-Mediated Inhibition of LTP in Tau(-/-) mice. *Front Neurosci,* 11**,** 201.

WONG, A. A. & BROWN, R. E. 2006. Visual detection, pattern discrimination and visual acuity in 14 strains of mice. *Genes Brain Behav,* 5**,** 389-403.

WU, H.-Y., KUO, P.-C., WANG, Y.-T., LIN, H.-T., ROE, A. D., WANG, B. Y., HAN, C.-L., HYMAN, B. T., CHEN, Y.-J. & TAI, H.-C. 2018. β-Amyloid Induces Pathology-Related Patterns of Tau Hyperphosphorylation at Synaptic Terminals. *Journal of Neuropathology & Experimental Neurology,* 77**,** 814-826.

WU, H. Y., HUDRY, E., HASHIMOTO, T., KUCHIBHOTLA, K., ROZKALNE, A., FAN, Z., SPIRES-JONES, T., XIE, H., ARBEL-ORNATH, M., GROSSKREUTZ, C. L., BACSKAI, B. J. & HYMAN, B. T. 2010. Amyloid beta induces the morphological neurodegenerative triad of spine loss, dendritic simplification, and neuritic dystrophies through calcineurin activation. *J Neurosci,* 30**,** 2636-49.

YASUDA, M. & MAYFORD, M. R. 2006. CaMKII activation in the entorhinal cortex disrupts previously encoded spatial memory. *Neuron,* 50**,** 309-18.

YEH, F. L., WANG, Y., TOM, I., GONZALEZ, L. C. & SHENG, M. 2016. TREM2 Binds to Apolipoproteins, Including APOE and CLU/APOJ, and Thereby Facilitates Uptake of Amyloid-Beta by Microglia. *Neuron,* 91**,** 328-40.

YETMAN, M. J., FOWLER, S. W. & JANKOWSKY, J. L. 2016. Humanized Tau Mice with Regionalized Amyloid Exhibit Behavioral Deficits but No Pathological Interaction. *PLOS ONE,* 11**,** e0153724.

YIN, Y., GAO, D., WANG, Y., WANG, Z. H., WANG, X., YE, J., WU, D., FANG, L., PI, G., YANG, Y., WANG, X. C., LU, C., YE, K. & WANG, J. Z. 2016. Tau accumulation induces synaptic impairment and memory deficit by calcineurin-mediated inactivation of nuclear CaMKIV/CREB signaling. *Proc Natl Acad Sci U S A,* 113**,** E3773-81.

ZEMPEL, H., THIES, E., MANDELKOW, E. & MANDELKOW, E.-M. 2010. A{beta} Oligomers Cause Localized Ca2+ Elevation, Missorting of Endogenous Tau into Dendrites, Tau Phosphorylation, and Destruction of Microtubules and Spines. *J. Neurosci.,* 30**,** 11938-11950.

ZERBINO, D. R., ACHUTHAN, P., AKANNI, W., AMODE, M. R., BARRELL, D., BHAI, J., BILLIS, K., CUMMINS, C., GALL, A., GIRON, C. G., GIL, L., GORDON, L., HAGGERTY, L., HASKELL, E., HOURLIER, T., IZUOGU, O. G., JANACEK, S. H., JUETTEMANN, T., TO, J. K., LAIRD, M. R., LAVIDAS, I., LIU, Z., LOVELAND, J. E., MAUREL, T., MCLAREN, W., MOORE, B., MUDGE, J., MURPHY, D. N., NEWMAN, V., NUHN, M., OGEH, D., ONG, C. K., PARKER, A., PATRICIO, M., RIAT, H. S., SCHUILENBURG, H., SHEPPARD, D., SPARROW, H., TAYLOR, K., THORMANN, A., VULLO, A., WALTS, B., ZADISSA, A., FRANKISH, A., HUNT, S. E., KOSTADIMA, M., LANGRIDGE, N., MARTIN, F. J., MUFFATO, M., PERRY, E., RUFFIER, M., STAINES, D. M., TREVANION, S. J., AKEN, B. L., CUNNINGHAM, F., YATES, A. & FLICEK, P. 2018. Ensembl 2018. *Nucleic Acids Res,* 46**,** D754-D761.

ZHOU, L., MCINNES, J., WIERDA, K., HOLT, M., HERRMANN, A. G., JACKSON, R. J., WANG, Y. C., SWERTS, J., BEYENS, J., MISKIEWICZ, K., VILAIN, S., DEWACHTER, I., MOECHARS, D., DE STROOPER, B., SPIRES-JONES, T. L., DE WIT, J. & VERSTREKEN, P. 2017. Tau association with synaptic vesicles causes presynaptic dysfunction. *Nat Commun,* 8**,** 15295.

KEY RESOURCES TABLE

REAGENT or RESOURCE	SOURCE	IDENTIFIER
Antibodies		
AW7 antibody, recognises amyloid beta, polyclonal, raised in rabbit	provided by Prof Dominic Walsh	N/A
PHF1 antibody, recognises human tau phosphorylated at Ser396/Ser404, mouse monocolnal IgG1	provided by Prof Peter Davies	N/A
Alz50 antibody, recognises human tau folded to bring amino acids 2-10 and 312-342 into proximity, mouse IgM	provided by Prof Peter Davies	N/A
AT8 antibody, recognises human tau phosphorylated at Ser202, Thr205, Mouse monoclonal IgG1	Thermo Fisher	RRID:AB_223647
Iba1antibody, Goat polyclonal	Abcam	RRID:AB_2224402
GFAP antibody, Rabbit polyclonal	DAKO	RRID:AB_10013382
PSD95 antibody, rabbit monoclonal	Cell signaling	RRID:AB_2292883
Tau antibody, goat polyclonal	R&D Systems	RRID:AB_573209
synaptophysin antibody, mouse monoclonal	Abcam	RRID:AB_2198854
Tau antibody Tau13, recognises human tau aa15-25, mouse monoclonal	Covance	RRID:AB_291452
Biological Samples		
Human Brain Tissue samples	Edinburgh Sudden Death Brain Bank or the Massachusetts General Hospital Alzheimer's Disease Research Centre Brain Bank	Case IDs found in Table 1
Chemicals, Peptides, and Recombinant Proteins		
LR White Medium Grade Acrylic Resin	Agar Scientific	Cat#R1281
Paraformeldahyde 16%	Agar Scientific	Cat#R1026
Tris buffered saline 10x	Fisher BioReagents	Cat#BP2471-1
Sucrose	Sigma Life Sciences	Cat#S0389-1KG
Thioflavin S	Fisher Scientific	Cat#15537519
Critical Commercial Assays		
Tau ELISA	Thermo Fisher Scientific	Cat#KHB0041
Amyloid beta 1-42 ELISA	Thermo Fisher Scientific	Cat#KHB3441
Deposited Data		
See associated excel spreadsheets in supplemental data Tables S1-S4		
Experimental Models: Organisms/Strains		
mouse: B6C3-Tg(APPsw,PSEN1dE9)85DboMm	Jackson Labs	Jax 34829
mouse: FVB.*Mapt*$^{tm1(EGFP)Klt}$	George Carlson, collaborator	N/A
mouse: B6.Cg-(Camk2a-tTA)1/MmayDboJ	George Carlson, collaborator	N/A
mouse: FVB-Tg(tetO-0N4R-MAPTwt)21221	George Carlson, collaborator	N/A
Oligonucleotides		

See table S5		
Software and Algorithms		
Fiji (Image J) v2.0.0	Open Source NIH software	
MATLAB v 2018b	Mathworks	
R package version 2.30.1	r-project free software	
Ingenuity Pathway Analysis v01-14	Qiagen	
Graphpad Prism v7.0d	Graphpad	
SPSS Statistics v24	IBM	
Custom imageJ and MATLAB macros used for image analysis are freely available on the University of Edinburgh Data Sharing repository	https://doi.org/10.7488/ds/2592	

Figure 1

Click here to access/download;Figure;Fig1.tif

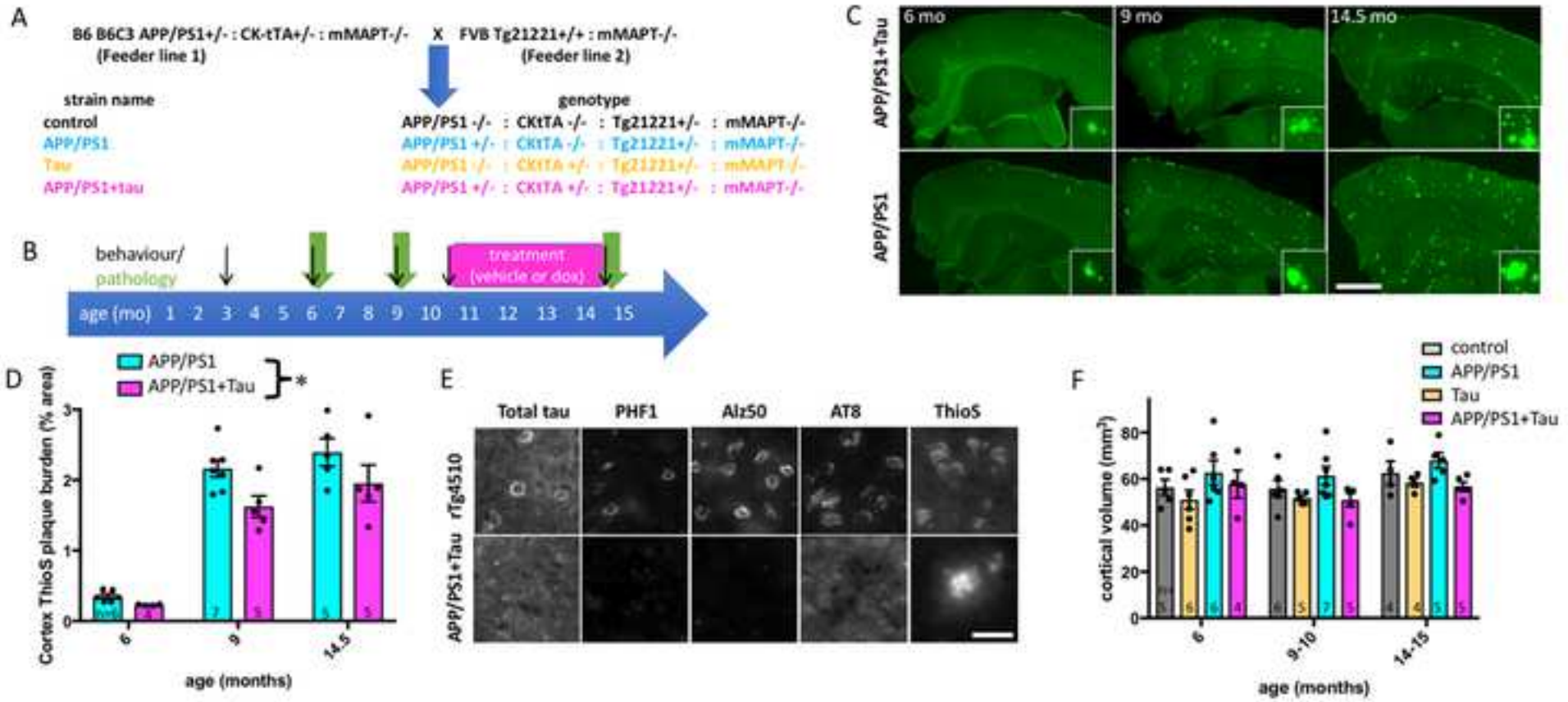

Figure 2

Click here to access/download;Figure;Fig2.tif

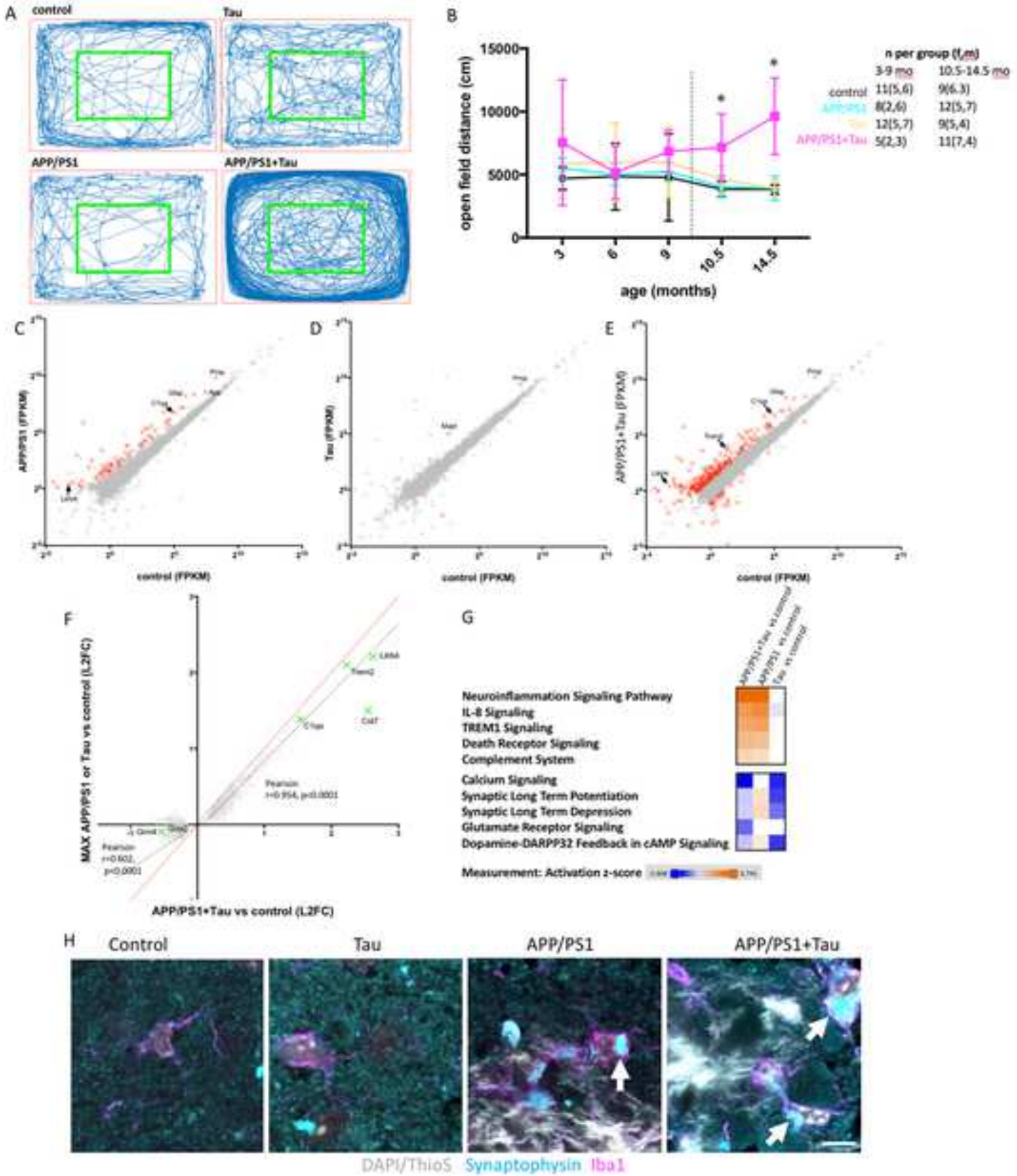

Figure 3

Click here to access/download;Figure;Fig3.tif

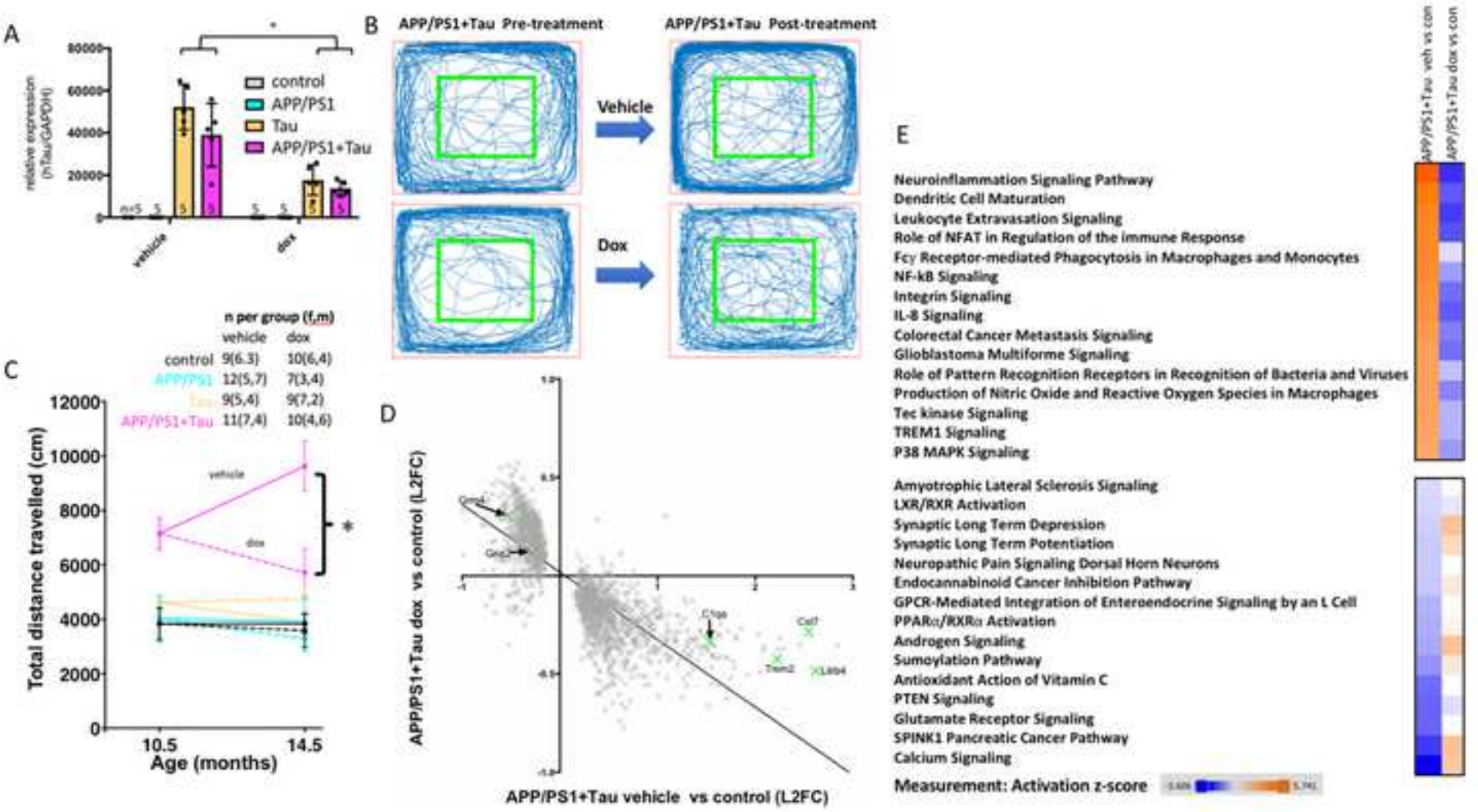

Figure 4

Click here to access/download;Figure;Fig4.tif

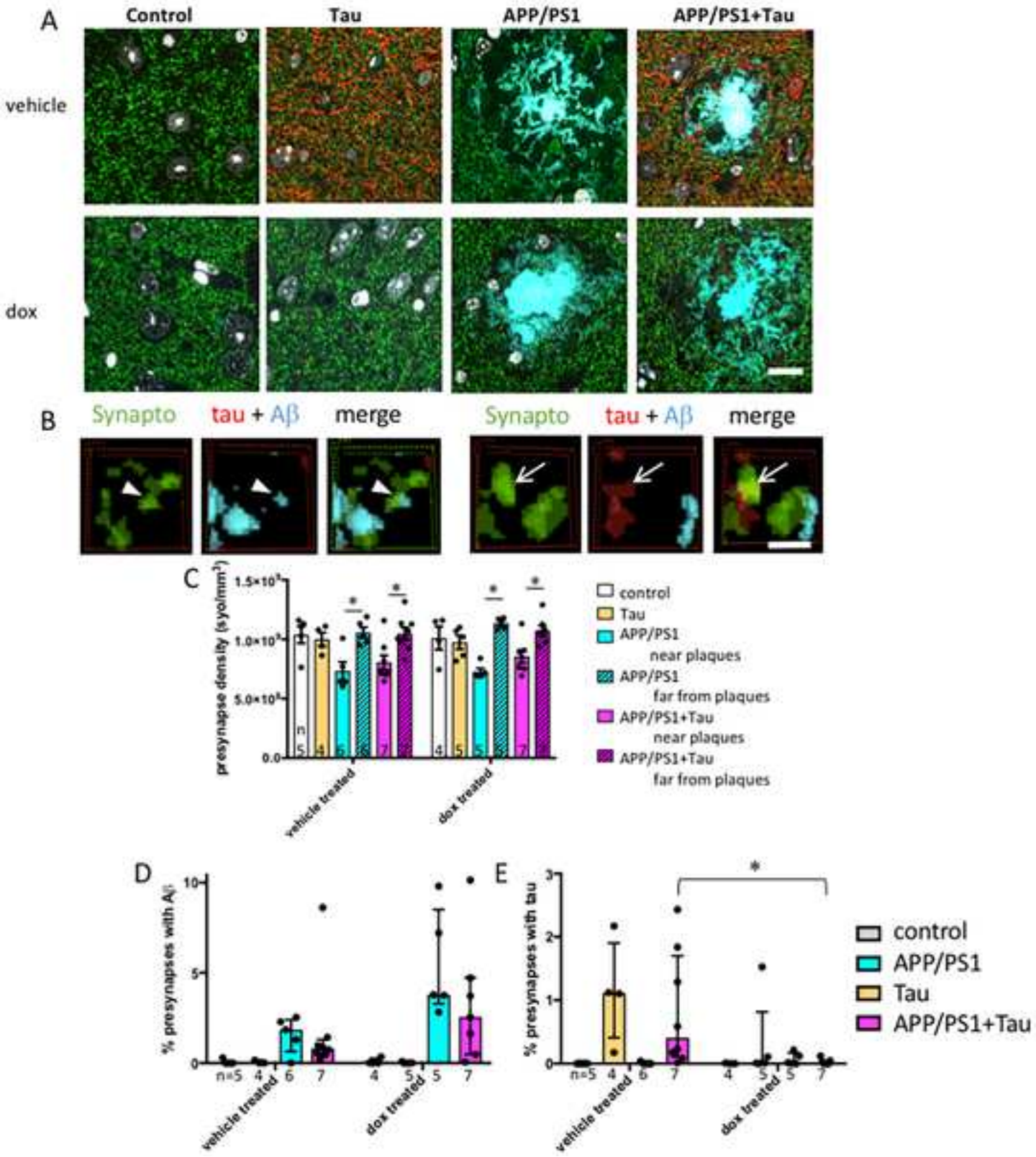

Figure 5

Click here to access/download;Figure;Fig5.tif

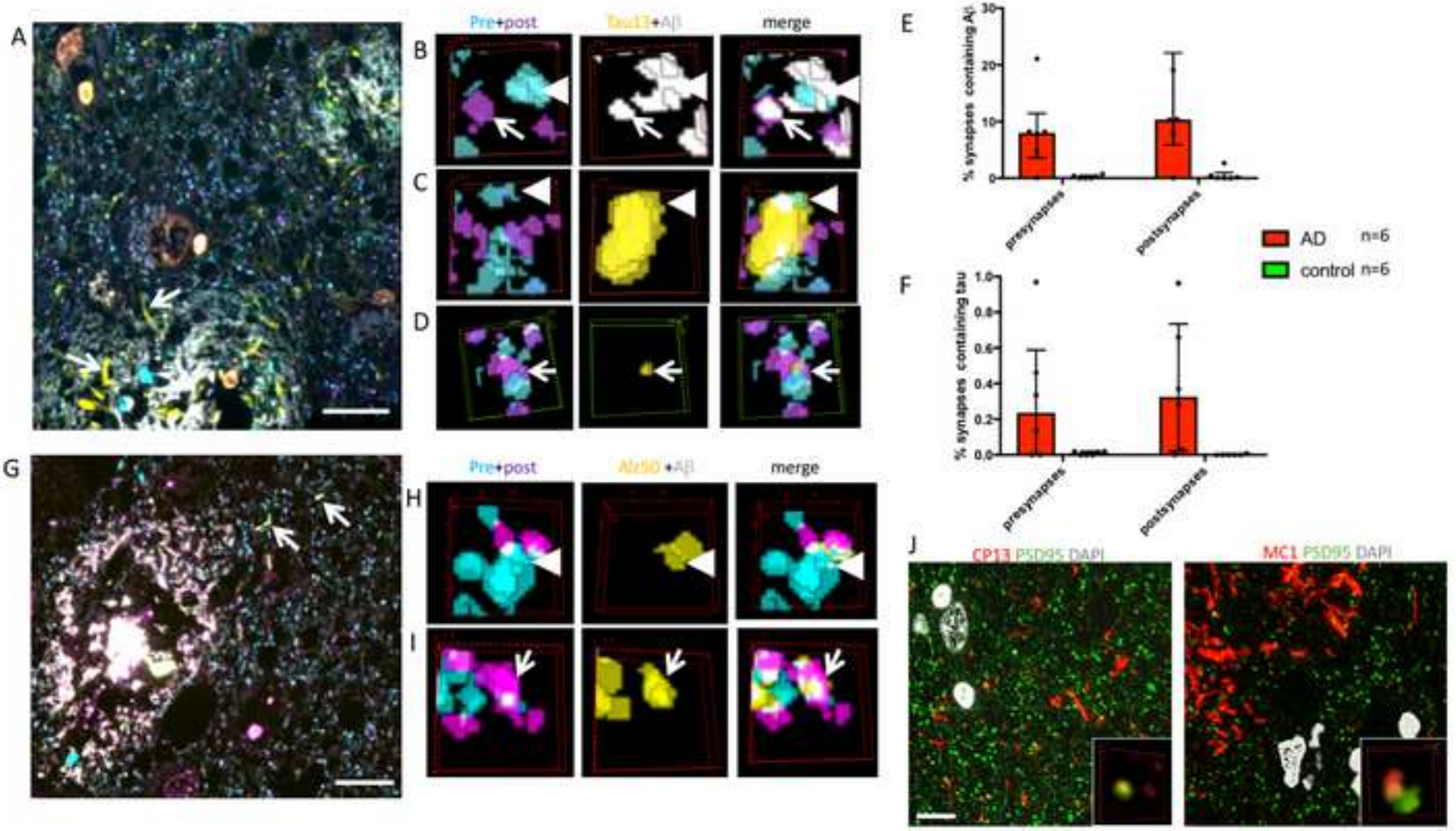

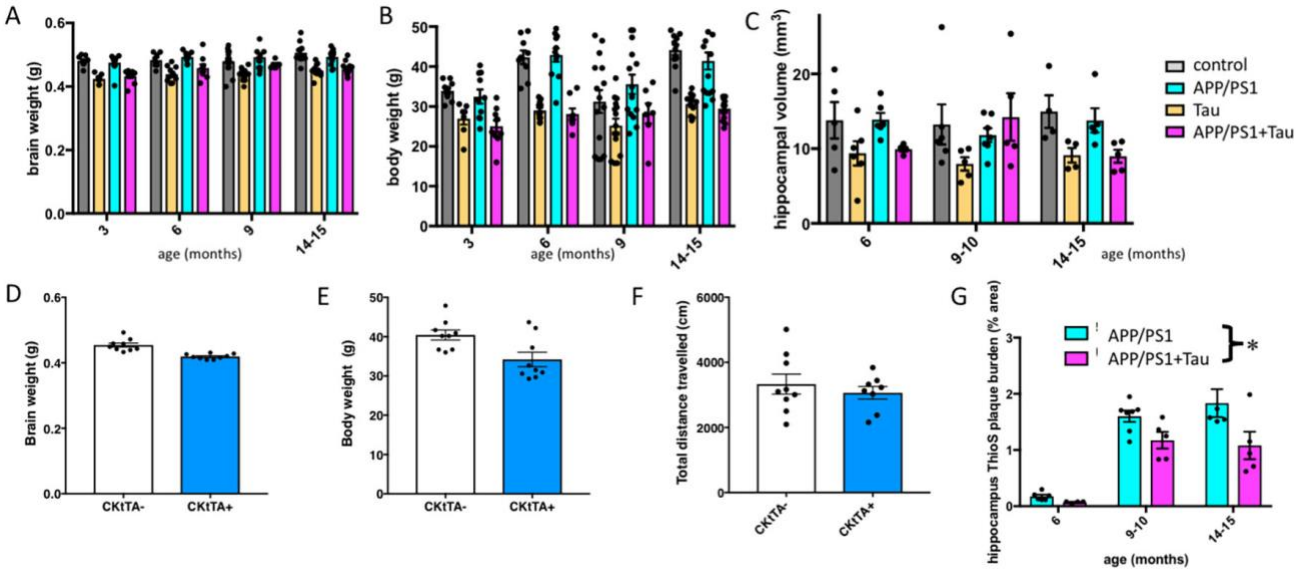

Figure S1 related to Figure 1: No age-related loss of brain, weight, body weight, or hippocampal volume in APP/PS1+Tau mice. There was a significant effect of genotype on brain weight (A, $F[3,163]=40.28$, $p<0.0001$), body weight B, $F[3,153]=37.25$, $p<0.001$), and hippocampal volume (C, $F[3,50]=4.82$, $p=0.005$) with both tau mice and APP/PS1+Tau mice exhibiting reductions compared to the other 2 genotypes. Despite reduced hippocampal volume in both APP/PS1+Tau and Tau mice, there was no age-related reduction in hippocampal volume (C, 2-way ANOVA effect of age $F[3,50]=0.002$, $p=0.997$). The reduction in brain and body weight is driven not by tau expression but by the CKtTA activator transgene that is needed to drive the tau transgene. 9 month old MAPTnullxCKtTA mice in the absence of the Tg21221 responder transgene have reduced brain (D, unpaired t-test $t=5.144$ $df=16$, $p<0.0001$) and body weights (E, unpaired t-test $t=2.803$ $df=16$, $p=0.012$). This loss of brain and body weight did not affect total distance travelled in the open field (F). Similar to the cortical data presented in Fig 1, hippocampal plaque burden was significantly smaller in APP/PS1+Tau mice compared to APP/PS1 mice (G, 2-way ANOVA effect of genotype $F[1,26]=11.21$, $p=0.002$, effect of age $F[2,26]=44.19$, $p<0.0001$).

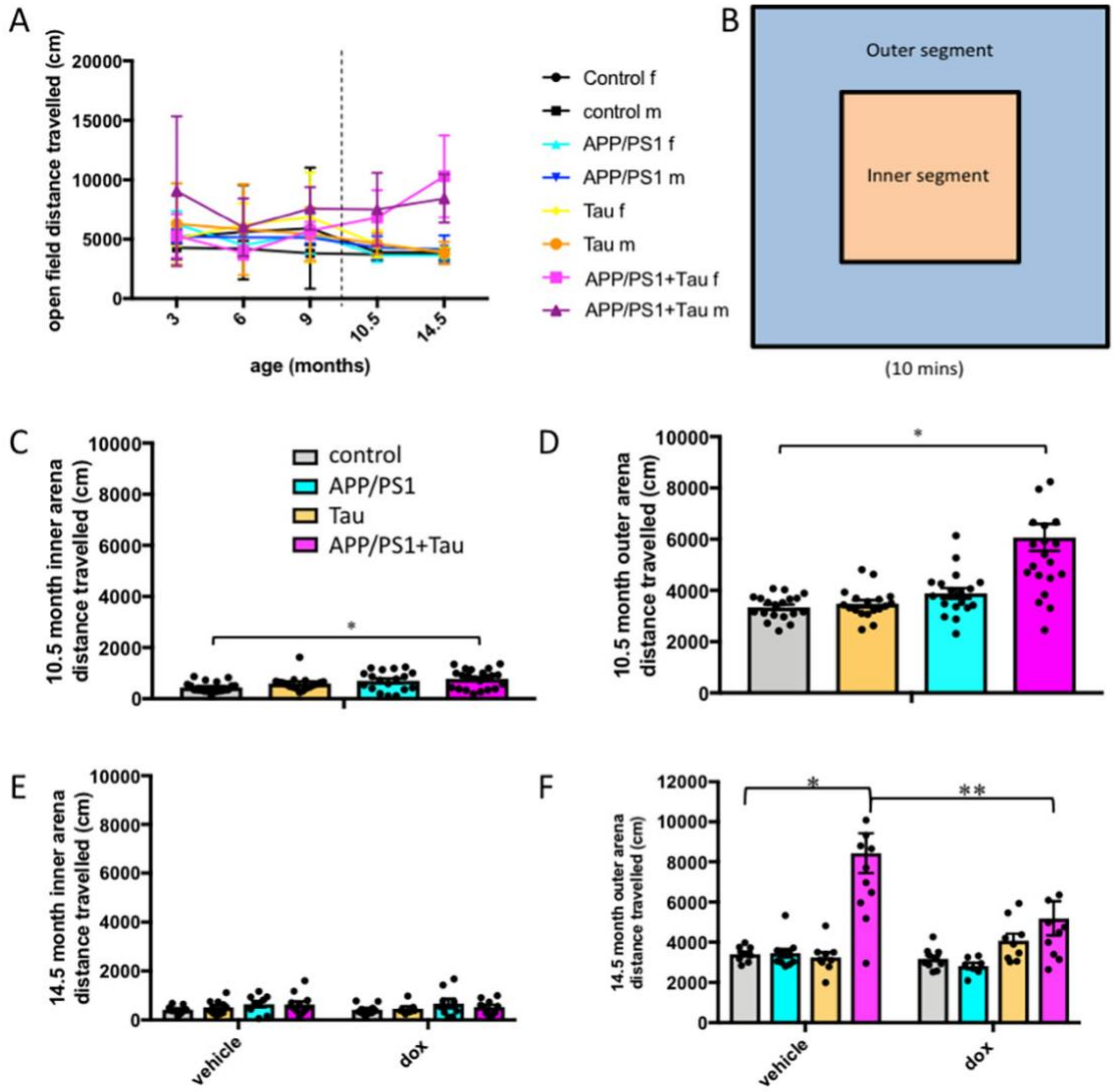

Figure S2 related to Figure 2: Hyperactivity is not different between male and female mice and open field data indicate anxiety in APP/PS1+Tau mice. The hyperactivity phenotype observed in APP/PS1+Tau mice is not different between male and female mice (A, one-Way ANOVA effect of sex $p>0.05$ at all age groups). To determine whether APP/PS1+Tau mice have an anxiety phenotype, open field data was analysed by the distance travelled in the inner segment versus outer segment of the arena (B). At 10.5 months, there was a significant difference between genotypes in the inner (C, ANOVA, $F[3,69]=4.075$, $p=0.010$) and outer (D, ANOVA $F[3,69]=15.91$, $p<0.0001$) portions of the arena. APP/PS1+Tau mice travelled significantly further in both the inner and outer arena compared to MAPTnull mice (* Tukey's posthoc test $p<0.01$). At 14.5 months, there were no significant differences between genotype and treatment in distance travelled in the inner arena (E). At 14.5 months of age, APP/PS1+Tau mice travel over 2 times farther in the outer portion of the arena (F) than other genotypes, a phenotype which recovers with dox treatment (2-way ANOVA genotype $F[3,69]=19.548$, $p<0.0001$; treatment $F[1,69]=3.9990$, $p=0.0497$, interaction $F[2,69]=4.770$, $p=0.004$. *, ** Tukey's multiple comparisons tests $p=0.002$, $p<0.0001$). Graphs depict mean ± SEM. Individual points represent the mean value for each mouse. The dotted line in A indicates that a different cohort of mice was used at 3,6, 9 months of age and at 10.14 months of age.

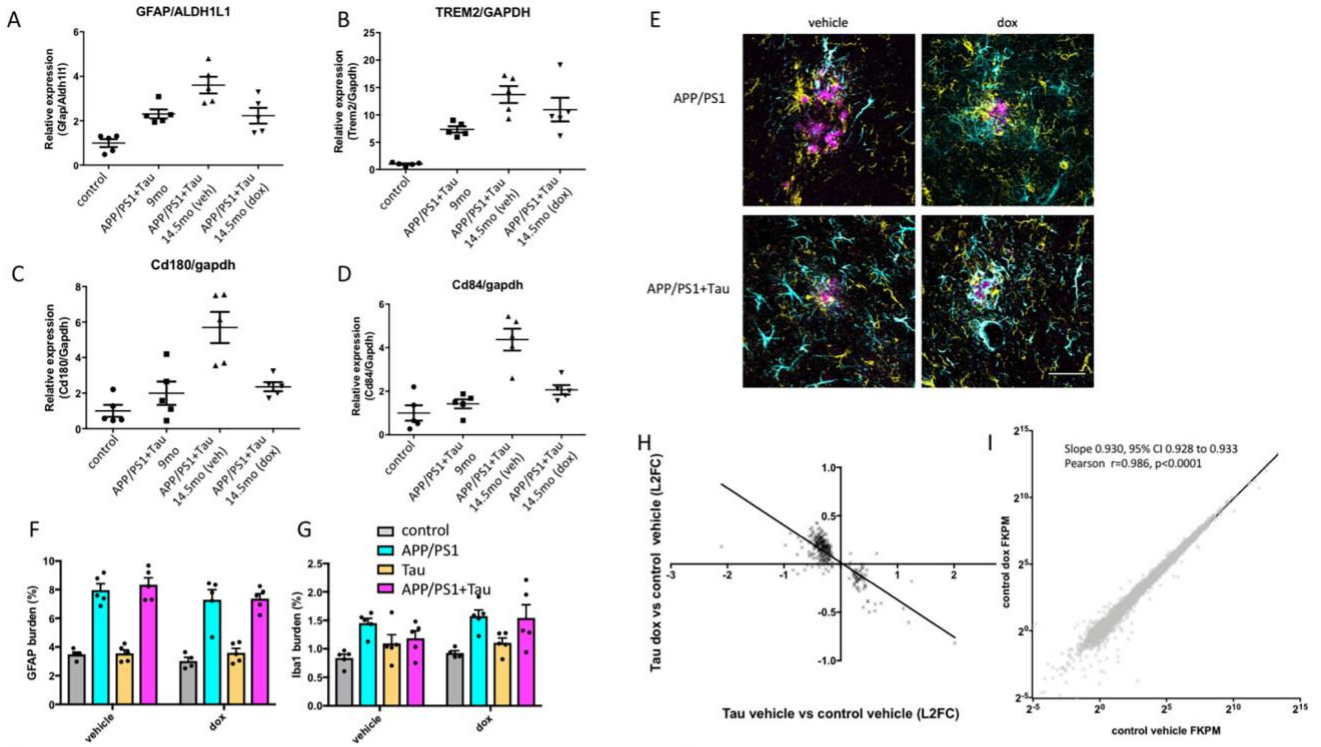
A
GFAP/ALDH1L1
Relative expression (GfapAldh1l1)
control
APP/PS1+Tau 9mo
APP/PS1+Tau 14.5mo (veh)
APP/PS1+Tau 14.5mo (dox)
B
TREM2/GAPDH
Relative expression (Trem2/Gapdh)
C
Cd180/gapdh
Relative expression (Cd180/Gapdh)
D
Cd84/gapdh
Relative expression (Cd84/Gapdh)
E
vehicle
dox
APP/PS1
APP/PS1+Tau
F
GFAP burden (%)
vehicle
dox
G
control
APP/PS1
Tau
APP/PS1+Tau
Iba1 burden (%)
H
Tau dox vs control vehicle (L2FC)
Tau vehicle vs control vehicle (L2FC)
I
Slope 0.930, 95% CI 0.928 to 0.933
Pearson r=0.986, p<0.0001
control dox FKPM
control vehicle FKPM

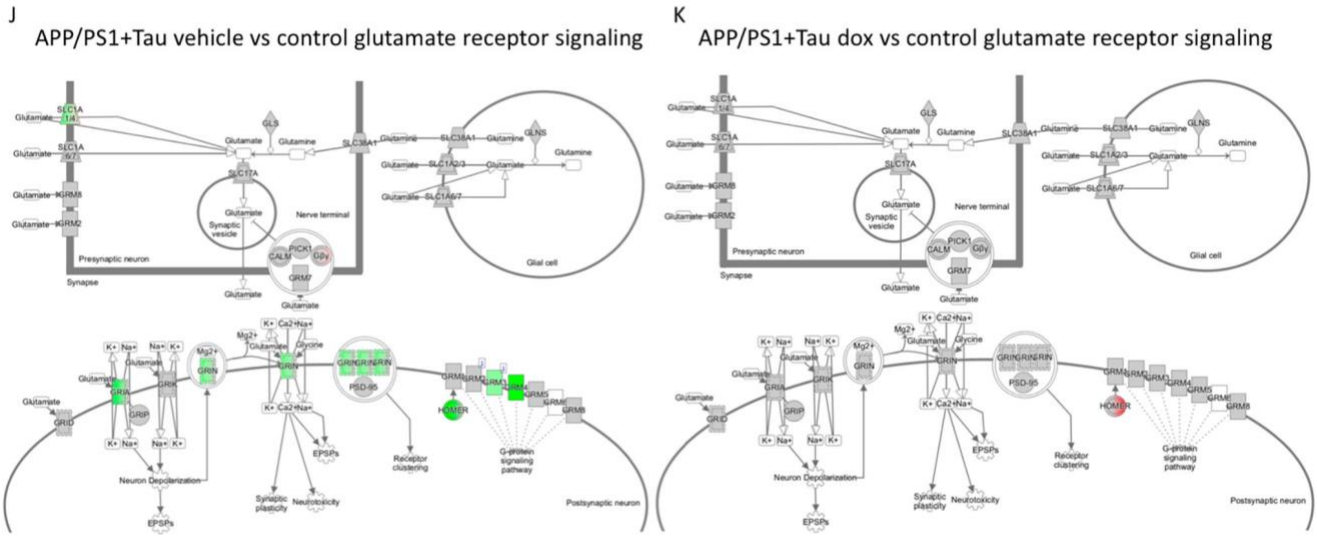
J
APP/PS1+Tau vehicle vs control glutamate receptor signaling
K
APP/PS1+Tau dox vs control glutamate receptor signaling
Glutamate
Glutamine
Presynaptic neuron
Synapse
Glial cell
Nerve terminal
Synaptic vesicle
Postsynaptic neuron
Neuron Depolarization
EPSPs
Synaptic plasticity
Neurotoxicity
Receptor clustering
G-protein signaling pathway
PSD-95
HOMER

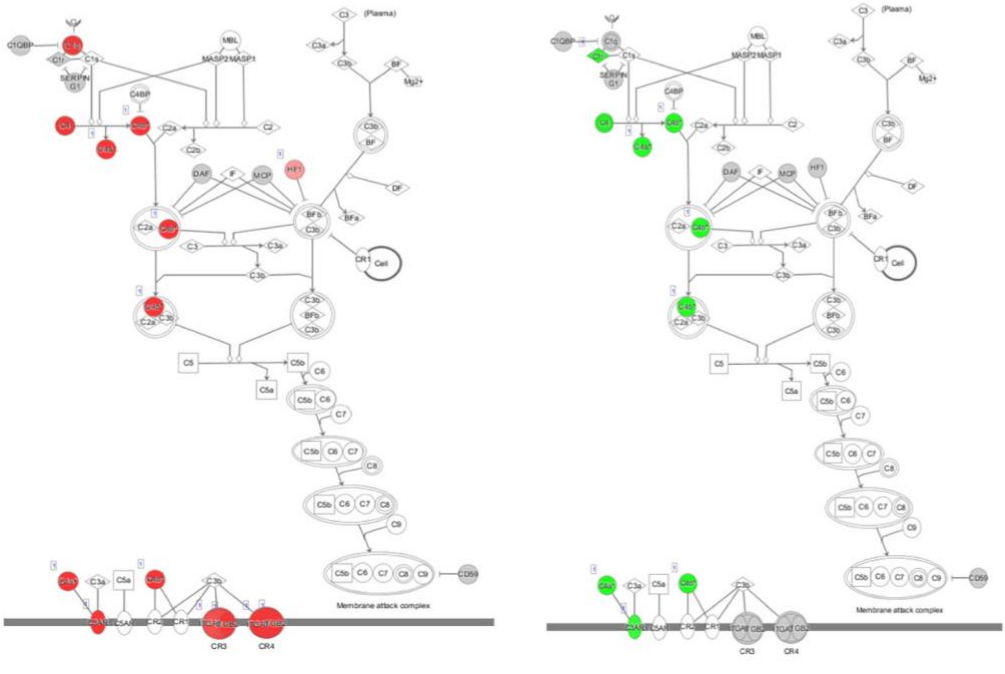
L
APP/PS1+Tau vehicle vs control complement system
M
APP/PS1+Tau dox vs control complement system
Membrane attack complex
CR3
CR4

Figure S3 related to Figure 3: RT-PCR validation of RNA-seq results at 9 months and 14.5 months of age indicate that the upregulated genes GFAP (A), Trem2 (B), Cd180 (C), and Cd84 (D) increase between 9 and 14.5 months and that this is prevented by dox treatment. The percentage area occupied by GFAP labelled astrocytes (cyan, E) and Iba1 labelled microglia (magenta E) was higher in 14.5 month old mice in genotypes with plaques but did not change with tau transgene suppression (F, GFAP 2-way ANOVA effect of genotype $F[3,31]=75.16$, $p<0.001$, treatment $F[1,31]=3.22$, $p=0.082$; G, Iba1 2-qay ANOVA effect of genotype $F[3.31]=9.05$, $p=0.0002$, treatment $F[1,31]2.48$, $p=0.13$). Dox treatment significantly rescues transcriptional changes in Tau mice at 14.5 months (H) without affecting control mice (I). Dox treated control data correlate very closely with values from vehicle treated control animals (J). To visualise recovery of networks with dox treatment, the changes in APP/PS1+Tau vehicle treated mice compared to controls are shown for glutamate signalling (j) and complement system (l) and dox treated APP/PS1+Tau mice compared to controls are shown in k and m. Transcripts labelled in red are increased and those labelled in green are decreased. Scale bar represents 40 μm.

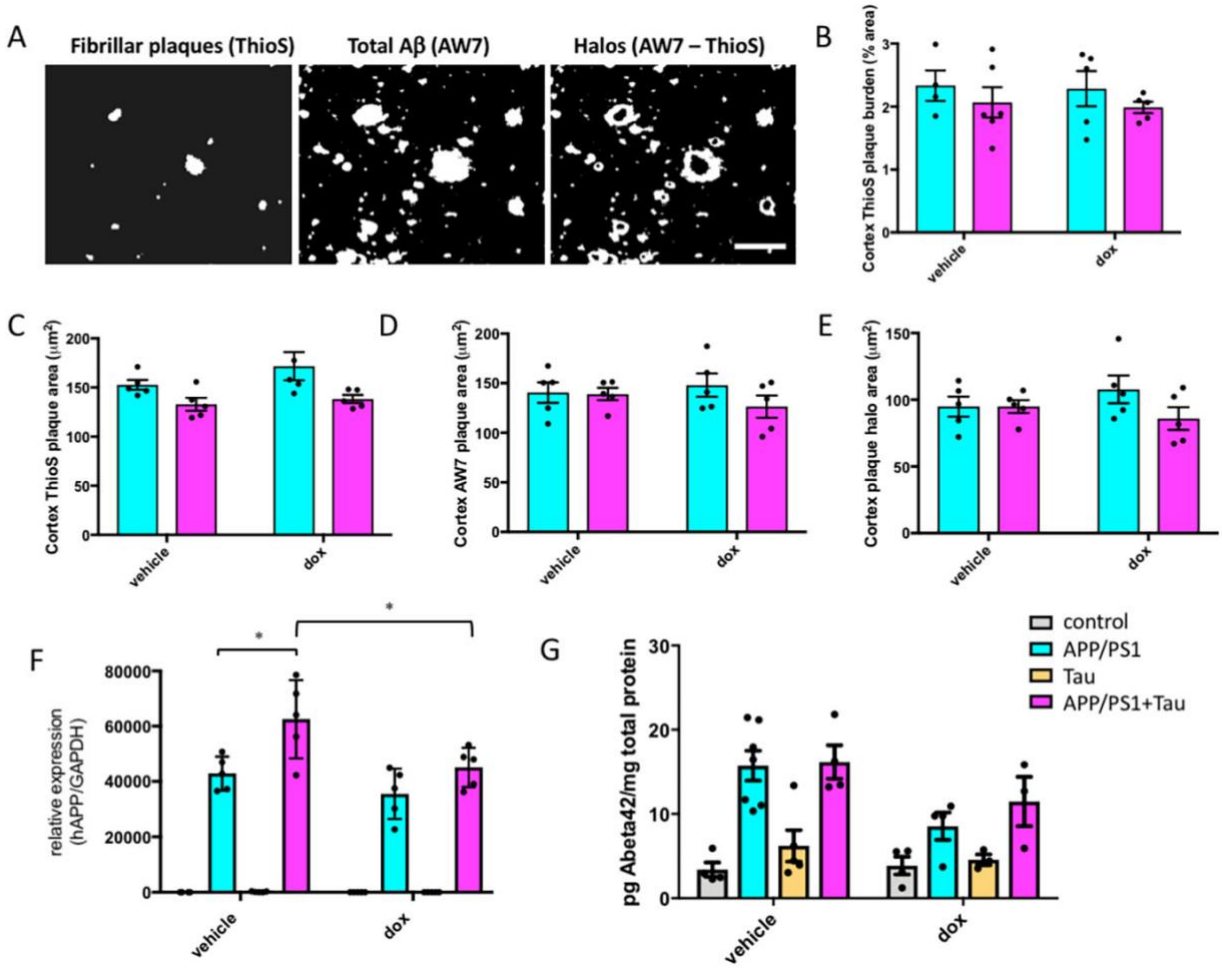

Figure S4 related to Figures 3 and 4: Tau suppression does not affect amyloid pathology. Tau suppression did not change amyloid pathology in APP/PS1+Tau mice. In 14.5 month old mice, fibrillar plaques were measured with ThioS, total Aß with AW7 immunostaining, and oligomeric Aß halos were measured by subtracting the fibrillar cores from total Ab staining (a). None of the amyloid plaque measurements was changed by doxycycline treatment (b-e). APP mRNA levels (f) were increased by 30% in APP/PS1+Tau mice, an effect which was ameliorated by dox treatment (2-way ANOVA genotype $F[3,31]=153.5$, $p<0.0001$, treatment $F[1,31]=7.912$, $p=0.0084$, interaction $F[3,31]=3.468$, $p=0.0279$, * post-hoc Tukey's test $p<0.01$). Soluble Aß42 ELISA on brain homogenates (g) showed a significant effect of genotype since mice without the human APP/PS1 transgene have low levels of Aß (2-way ANOVA effect of genotype $F[3,26]=13.14$, $p<0.0001$). There was a significant effect of dox treatment when all genotypes were considered (2-way ANOVA effect of treatment $F[1,26]=6.11$, $p=0.02$), however post-hoc analyses reveal that Aß42 levels were not changed in APP/PS1+Tau mice compared to APP/PS1 mice an neither APP/PS1+Tau nor APP/PS1 Aß42 levels were significantly reduced by dox treatment (Tukey's multiple comparisons tests $p>0.05$). Scale bar represents 30 μm.

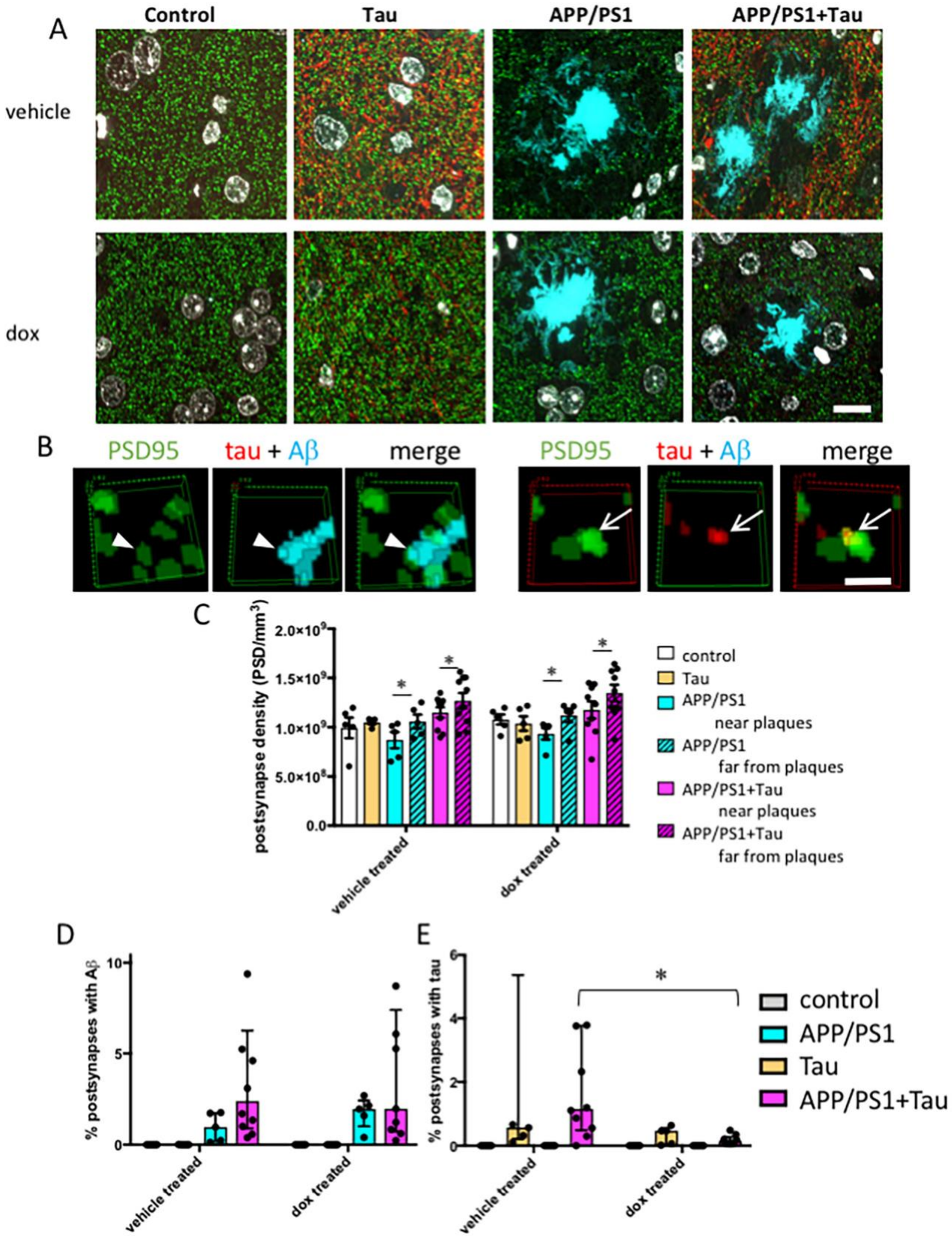

Figure S5 related to Figure 4: Tau suppression reduces post-synaptic accumulation of tau. To investigate post-synapse loss and synaptic proteins, array tomography ribbons from 14.5 month old mice were stained for postsynaptic terminals (green), human tau (red), and amyloid beta (AW7, cyan).

Maximum intensity projections of 10 serial 70 nm sections are shown in a. Three-dimensional reconstructions of 5 consecutive serial sections from processed image stacks of a APP/PS1+Tau mouse (b) demonstrate post-synaptic terminals positive for tau (arrows) or Aβ (arrowheads). Quantification reveals significant post-synapse loss near plaques in APP/PS1 and APP/PS1+Tau mice which is not rescued by lowering tau levels with doxycycline (dox) treatment (c). The percentage of post-synapses positive for Aβ is not different between APP/PS1 mice and APP/PS1+Tau mice, nor is it affected by dox treatment (d). The percentage of post-synapses containing tau is significantly lowered by dox treatment in APP/PS1+Tau mice (e, * Mann-Whitney U test p=0.004). Data represent mean + SEM (c) and median + interquartile range (d-e). Scale bars represent 10 μm in a, 1 μm in b.

Table S5 related to STAR methods - oligonucleotides

Genotyping primers
PSEN1dE9 forward primer: GGCTACCATTAAGTCAGTCAGCTTT
PSEN1dE9 reverse primer: CCCACAGTCTCGGTATCTTCTG
APPSwe forward primer: CCGACATGACTCAGGATATGAAGTT
APPSwe reverse primer: CCGACATGACTCAGGATATGAAGTT
CkTTA forward primer: TGCCAACAAGGTTTTTCACTAGAGA
CkTTA reverse primer: CTCTTGATCTTCCAATACGCAACCTA
MAPT forward primer: CTGCTCCAAGACCAAGAAGGA
MAPT reverse primer: TGTGTATGTCCACCCCACTGA
RNASeq validation QPCR primers
Gapdh forward primer: GGGTGTGAACCACGAGAAAT
Gapdh reverse primer: CCTTCCACAATGCCAAAGTT
MAPT forward primer: CCCAATCACTGCCTATACCC
MAPT reverse primer: CCACGAGAATGCGAAGGA
Human mutant *APP* forward primer: CCGACATGACTCAGGATATGAAGTT
Human mutant *APP* reverse primer: CCTTTGTTTGAAACCCACATCTTCTG
Trem2 forward primer: CTGGAACCGTCACCATCACTC
Trem2 reverse primer: CGAAACTCGATGACTCCTCGG
Gfap forward primer: GCAAAAGCACCAAAGAAGGGGA
Gfap reverse primer: ACATGGTTCAGTCCCTTAGAGG
Aldh1l1 forward primer: CATCCAGACCTTCCGATACTTC
Aldh1l1 reverse primer: ACAATACCACAGACCCCAAC
Cd180 forward primer: CCAAAGCCAACATCGGTTAGACAC
Cd180 reverse primer: CAGAGACCCTCAAACACGGCAGG
Cd84 forward primer: GCTGAAGTTACCATAACCCAGG
Cd84 reverse primer: CAAAAGTAAATCCAAGGCCCCG